

The benefits of increasing resolution in global and regional climate simulations for European climate extremes

Carley E. Iles¹, Robert Vautard¹, Jane Strachan², Sylvie Joussaume¹, Bernd R. Eggen² and Chris D. Hewitt²

¹Laboratoire des Sciences du Climat et de l'Environnement, LSCE-IPSL, CEA-CNRS-UVSQ, Université Paris-Saclay, F-91198 Gif-sur-Yvette, France

²Hadley Centre, Met Office, Exeter, UK

Correspondence to: Carley E. Iles (carley.iles@lsce.ipsl.fr)

Abstract. Many climate extremes, including heatwaves and heavy precipitation events, are projected to worsen under climate change, with important impacts for society. Future projections, required for adaptation, are often based on climate model simulations. Given finite resources, trade-offs must be made concerning model resolution, ensemble size and level of model complexity. Here we focus on the resolution component. A given resolution can be achieved over a region using either global climate models (GCMs) or at lower cost using regional climate models (RCMs) that dynamically downscale coarser GCMs. Both approaches to increasing resolution may better capture small-scale processes and features (downscaling effect), but increased GCM resolution may also improve the representation of the large-scale atmospheric circulation (upscaling effect). The size of this upscaling effect is therefore important for deciding modelling strategies. Here we evaluate the benefits of increased model resolution for both global and regional climate models for simulating temperature, precipitation and wind extremes over Europe at resolutions that could currently be realistically used for coordinated sets of climate projections at the pan-European scale. First we examine the benefits of regional downscaling by comparing EURO-CORDEX simulations at 12.5 and 50 km resolution to their coarser CMIP5 driving simulations. Secondly, we compare global scale HadGEM3-A simulations at three resolutions (130, 60 and 25 km). Finally, we separate out resolution dependent differences for HadGEM3-A into downscaling and upscaling components using a circulation analogue technique. Results suggest limited benefits of increased resolution for heatwaves, except in reducing hot biases over mountainous regions. Precipitation extremes are sensitive to resolution, particularly over complex orography, with larger totals and heavier tails of the distribution at higher resolution, particularly in the CORDEX vs CMIP5 analysis. CMIP5 models underestimate precipitation extremes, whilst CORDEX simulations overestimate compared to E-OBS, particularly at 12.5 km, but results are sensitive to the observational dataset used, with the MESAN reanalysis giving higher totals and heavier tails than E-OBS. Wind extremes are somewhat stronger and heavier tailed at higher resolution, except at coastal regions where large coastal grid boxes spread strong ocean winds further over land. The circulation analogue analysis suggests that differences with resolution for the HadGEM3-A GCM are primarily due to downscaling effects.

33 **1 Introduction**

34 Climate extremes, such as heatwaves and heavy precipitation events are projected to worsen under climate change,
35 with important impacts for society (Seneviratne et al., 2012). Such projections are generally based on numerical climate
36 model simulations. However, given finite computational resources, trade-offs between model resolution, ensemble size
37 and the level of model complexity are necessary. For extreme events driven by large-scale processes such as stationary
38 anticyclones, the proper simulation of the amplitude of extremes is limited by dynamics but also by land-atmosphere
39 feedbacks and the many physical processes involved in the surface energy budget. Such extremes are typically heat
40 waves, droughts and cold spells. Many other types of extreme event are by nature small scale, i.e. on the order of a
41 few kilometres to a few hundred kilometres. Such is the case of convective precipitation, flash floods, extratropical
42 wind storms, cyclones and medicanes. These are poorly resolved at the resolution of Global Climate Models (GCMs)
43 in CMIP5 (Coupled Model Intercomparison Project Phase 5; Taylor et al., 2012). Increased resolution in GCMs may
44 improve the representation of small-scale processes and features, including orography and coastlines (downscaling
45 effect), but potentially may also improve the representation of the interaction between small and large scale dynamical
46 processes and ultimately improve the large-scale atmospheric flow (upscaling effect). For instance, a better
47 representation of baroclinic eddies may help to better simulate large Rossby waves such as those inducing long-lived
48 anomalies, due to the inverse energy cascade. This may improve the simulation of the frequency and duration of heat
49 waves and cold spells, and related anomalies such as summer droughts. For precipitation and wind extremes, an
50 improvement with resolution could be expected due to the small-scale processes and features involved, including
51 convection and the influence of topography. However, upscaling effects may also have benefits by improving storm-
52 track location, and duration of wet spells. An alternative approach to increasing the resolution of global-scale models
53 is to use regional climate models (RCMs) driven by coarser GCMs to achieve a given high resolution over a limited
54 area at lower cost. However, this technique only captures downscaling effects, since the RCM inherits the large scale
55 circulation from the driving GCM.

56
57 Current generation GCMs commonly used for climate projections (e.g. CMIP5 models) have a horizontal grid spacing
58 ranging from about 70 to 250 km. Resolution has been increasing further in CMIP6 (Eyring et al. 2016), with some 25
59 km simulations now being run under projects such as PRIMAVERA and HighResMIP (part of CMIP6; Haarsma et
60 al., 2016). For coordinated RCM experiments, such as CORDEX (Coordinated Regional Downscaling Experiment;
61 Giorgi et al., 2009), grid spacing is generally between 10 to 50 km (e.g. Jacob et al., 2014). In order to simulate
62 convective precipitation a grid spacing of <5 km is needed, which is very computationally expensive, but such
63 ensembles of convection permitting RCMs are currently in development (e.g. Coppola et al., 2019; Risanto et al. 2019).
64 An important question is the extent to which increased resolution benefits the simulation of extreme events for both
65 global and regional models for the kind of resolutions that can realistically be run for coordinated pan-continental
66 climate projections. Particularly, whether using global high resolution adds further benefits over regional high
67 resolution due to an improved large scale circulation. We will address these questions focusing on Europe, for which
68 a large number of coordinated RCM simulations at two standard resolutions are available as part of the EURO-
69 CORDEX initiative (Jacob et al., 2014), and whose climate is highly variable and affected by a range of both large and

70 small scale processes, which present challenges for adequate simulation. We focus on extreme precipitation,
71 temperature and wind, to cover a range of phenomena that may be affected by resolution in different ways. Throughout
72 the rest of this manuscript we use the term “resolution” to mean model horizontal grid spacing, whilst recognising that
73 a model’s effective resolution, in terms of the scales it can capture, is always coarser than its grid spacing (Skamarock
74 2004; Klavar et al. 2020).

75
76 The benefits of increased resolution for European precipitation extremes are well documented, whilst the effects on
77 heatwaves, cold spells and wind extremes are less well known. In GCMs, global precipitation tends to increase with
78 resolution, and for grid point GCMs (as opposed to spectral GCMs) the fraction of land precipitation and moisture
79 fluxes from land to ocean increases, largely due to better resolved orography (Vannière et al., 2019; Terai et al., 2018;
80 Demory et al., 2014). Precipitation extremes tend to get heavier and in some studies agree better with observational
81 estimates with increased resolution (Wehner et al., 2010, O’Brien et al., 2016; Kopparla et al., 2013; Shields et al.,
82 2016; Vannière et al., 2019; Demory et al. 2020; Strandberg and Lind 2020), unless the parameterisation schemes are
83 not suited to the resolution (e.g. Wehner et al., 2014 and possibly Bador et al. 2020, who found worse performance in
84 higher resolution versions of multiple GCMs whose parameterisations were not retuned at higher resolution,
85 particularly in the tropics). In Europe, Schiemann et al. (2018) find that both mean and extreme precipitation are
86 simulated better with increased resolution in HadGEM3A, mostly originating from better resolved orography. In
87 contrast, Van Haren et al. (2015a) find that improvements in Northern and Central European mean and extreme winter
88 precipitation with resolution are mostly associated with improved storm tracks in EC-Earth. For RCMs, extreme
89 precipitation is improved with resolution when compared to high resolution observations, particularly over orography,
90 including frequency-intensity distributions and spatial patterns, (e.g. Torma et al., 2015; Prein et al., 2016; Ruti et al.,
91 2016; Fantini et al. 2018). However, benefits are smaller for regional and seasonal mean precipitation. Convection
92 permitting models (<4km grid spacing) are particularly beneficial in simulating summer extreme and sub-daily
93 precipitation, including the diurnal cycle of convection, but can overdo extreme precipitation (e.g. Prein et al., 2015;
94 Kendon et al., 2012; 2014).

95
96 For heatwaves, increasing horizontal resolution does not lead to obvious benefits in RCM simulations (see e.g. Vautard
97 et al., 2013 for EURO-CORDEX), except improved spatial detail (Gutjahr et al., 2016). However, increased resolution
98 may have more impact in global models since the large scale circulation that contributes to heatwave formation may
99 be affected. This remains a largely unstudied question, with the exception of a few studies such as Cattiaux et al. (2013)
100 who find that increasing resolution in the IPSL GCM leads to a reduction in the cold bias of both cold and warm
101 extremes in Europe, along with improved statistics, such as duration and frequencies and improved weather regimes.

102
103 For wind extremes, stronger winds and better spatial detail with resolution have been found for regional models (e.g.
104 Pryor et al., 2012; Kunz et al., 2010). Donat et al. (2010) found that observed storm loss estimates for Germany could
105 be reconstructed more accurately through dynamical downscaling compared to using the coarser resolution driving
106 ERA-40 data directly. Ruti et al., (2016) found improvements in Mediterranean cyclogenesis in coupled Med-
107 CORDEX RCMs relative to the ERA-interim driving data, whilst extreme winds over the Mediterranean generally

108 improve (i.e. are stronger) with higher resolution RCMs (e.g. Ruti et al. 2016; Hermann et al. 2011). Most GCM studies
109 focus on the simulation of extratropical cyclones rather than wind directly. Such studies find an improvement in the
110 representation of various aspects of Northern Hemisphere extratropical cyclones with increased resolution, including
111 frequency, intensity and the position of the storm tracks (Colle et al., 2013; Jung et al., 2006; 2012), even in the higher
112 resolution CMIP5 models ($\sim < 130$ km; Zappa et al., 2013). Vries et al., (2019) found that the resolution of Atlantic
113 Gulf-Stream SST fronts affects winter extratropical cyclone strength. Gao et al (2020) found that explosively
114 intensifying “bomb” extratropical cyclones are more frequent and associated with stronger winds in higher resolution
115 GCMs. Whether the aforementioned improvements translate into an improvement in wind extremes remains to be
116 assessed.

117
118 Persistence of weather regimes, such as blocking or the phase of the North Atlantic Oscillation, can be important
119 drivers for extreme events in Europe. Using the ECMWF IFS model, Dawson et al., (2012; 2015) find that such weather
120 regimes cannot be simulated realistically at typical CMIP5 resolution (~ 125 km grid spacing), but are improved at 40
121 km, and well-simulated at 16 km. Cattiaux et al., (2013) find improvements at more modest resolutions in the IPSL
122 model. However, multi model GCM analyses by Strommen et al. (2019) and Fabiano et al. (2020) suggest that only
123 some aspects of weather regimes are systematically improved with resolution, and that these aspects are not consistent
124 between atmosphere only or coupled GCMs. Blocking frequency tends to be underestimated by CMIP5-resolution
125 climate models (Anstey et al., 2013). This tends to be somewhat improved with resolution, particularly over the North
126 Atlantic (Jung et al., 2012, Anstey et al., 2013; Matsueda et al., 2009, Berckmans et al., 2013, Davini et al., 2017a;
127 2017b; 2020; Strommen et al. 2019; Schiemann et al. 2020), although results tend to be somewhat sensitive to season
128 and model considered (Schiemann et al., 2017) and compensating errors may be involved (Davini et al., 2017a for EC-
129 EARTH). O’Reilly et al. (2016) find that having a well-resolved Gulf stream SST front is also important for European
130 winter blocking and associated cold spells. An important question is whether these improvements in the large scale
131 circulation translate into an improvement in the simulation of European climate extremes.

132
133 Here we examine the benefits of increased resolution for global and regional models for the simulation of European
134 temperature, precipitation and wind extremes. We further break down any resolution related differences for a global
135 model into upscaling and downscaling components. This will shed light on whether potential improvements in the
136 large scale circulation suggested in the literature translate into an improved representation of climate extremes. This is
137 an important consideration in choosing how to distribute finite resources between global and regional models. We
138 focus on the kind of models widely used to provide climate projections at a European scale, applying a consistent
139 approach across model types. Firstly, the benefits of regional dynamical downscaling are explored by comparing
140 EURO-CORDEX simulations at 50 and 12.5 km resolutions to their coarser driving CMIP5 GCMs. Secondly, the
141 benefits of increased resolution for a global model are examined using HadGEM3-A at 130, 60 and 25 km resolution.
142 Finally, the roles of upscaling versus downscaling will be examined using a circulation analogue technique applied to
143 HadGEM3-A.

144 **2 Observational and model data**

145 **2.1 Observational data**

146 Model simulations are evaluated using observational and reanalysis datasets. For daily precipitation and daily
147 maximum temperature, we use the gridded station based dataset E-OBS v15 on a 0.5° latitude-longitude grid (Haylock
148 et al. 2008). This covers the European domain from 1950 to present. Gridded datasets tend to reduce the magnitude of
149 extremes compared to station data through smoothing effects, but are more comparable to the grid box averages from
150 GCMs (Haylock et al. 2008). E-OBS has a somewhat non-uniform underlying station density, with relatively high
151 densities in Germany, Sweden and Slovenia, and low densities in other countries (e.g. Spain, France, Austria). It tends
152 to underestimate precipitation extremes relative to higher density regional datasets, especially where it has poor
153 coverage, due to missed extremes which are local in scale (Prein and Gobiet 2017; Herrera et al. 2019). However, such
154 high resolution datasets are not available at a pan-European scale. As a compromise, results are repeated for
155 precipitation extremes using the 5.5 km resolution MESAN reanalysis (Landelius et al. 2016), which adjusts a
156 downscaled first guess from the 22km resolution HIRLAM reanalysis (Dahlgren et al. 2016) with a network of station-
157 based precipitation observations. For much of Europe these are the same as those used for E-OBS, but with the addition
158 of Swedish Meteorological and Hydrological Institute (SMHI) stations over Sweden, and a high density of Meteo-
159 France stations over France (Landelius et al. 2016). MESAN provides daily precipitation data for the more limited
160 period 1989-2010. Prein and Gobiet (2017) find that it gives heavier extremes than E-OBS in some regions (France,
161 Spain, the Carpathians), but generally not as high as the high resolution regional datasets (except in France). Neither
162 dataset is corrected for gauge undercatch, which tends to be around 3-20% for rain, and up to 40% for snow, or even
163 80% for non-shielded gauges (Førland and Institutt 1996; Goodison et al. 1997).

164
165 Wind extremes tend to happen on sub-daily time scales, necessitating the use of sub-daily data to avoid missing as
166 many events (although events, or their peak magnitude, will still be missed). We use 10 m wind speed from three
167 reanalysis datasets. These are the EURO4M DYNAD (Landelius et al. 2016), UERRA MESCOAN-SURFEX (Bazile et
168 al. 2017) and ERA5 (Hersbach et al. 2019) reanalyses. The former is available at 6 hourly intervals on a 5.5km rotated
169 grid over Europe for the period 1979-2013 and is computed through dynamical adaptation of a downscaled version of
170 the 22km resolution HIRLAM reanalysis to 5.5 km resolution orography using DYNAD (a simplified version of
171 HIRLAM). MESCOAN is also available at the same spatial and temporal resolution over Europe from 1961 onwards,
172 but is computed through dynamical downscaling of the 11 km UERRA-HARMONIE reanalysis. Both HIRLAM and
173 UERRA-HARMONIE are forced by the ERA interim global reanalysis (ERA40 before 1979 for the latter). Finally,
174 ERA5 is available globally at 0.25° and at hourly resolution from 1979 onwards. We sub-sample ERA5 to 6 hourly
175 data by taking every sixth value in order to be consistent with the other reanalyses.

176

177 **2.2 Climate model data**

178 **2.2.1 EURO-CORDEX and CMIP5**

179 In order to examine the effect of dynamical downscaling for climate extremes, we make use of the EURO-CORDEX
180 (Jacob et al. 2014) RCM simulations for the historical period over the European domain which are driven by lower
181 resolution global scale coupled CMIP5 GCMs. The GCMs are forced by observed records of anthropogenic and natural
182 forcings, such as greenhouse gases, anthropogenic aerosols, land use changes, solar variability and volcanic aerosols
183 to allow comparability to historical records. For the most part the RCMs inherit the effects of these forcing agents from
184 the GCMs, with the exception of greenhouse gases, which are prescribed. A comparison of the RCM simulations with
185 their driving CMIP5 simulations allows us to identify any value added by regional high resolution. The EURO-
186 CORDEX simulations are available at 0.11° and 0.44° (12.5 km and 50 km respectively), allowing an assessment of
187 the difference that increased regional resolution brings. Simulations are performed with the same model versions and
188 parameterisations for both resolutions, except for REMO where rain advection is used at 0.11° but not 0.44° (Kotlarski
189 et al. 2014). By examining the subset of GCM-RCM combinations that are common to both CORDEX resolutions
190 along with their driving GCMs we can isolate the effects of changing resolution. Hereafter, this subset is referred to as
191 the “common subset”. We also examine how representative the results for this common subset are by recalculating
192 them using all available CMIP5 and CORDEX simulations, using one member per model.

193
194 Daily precipitation (pr), daily maximum temperature (tasmax), and 3 hourly wind (sfcWind) were taken from both
195 CORDEX and CMIP5. For wind, every other time step was taken in order to obtain 6 hourly data to be consistent with
196 the reanalysis data. The simulations used are shown in Table S1. These consist of 23 and 19 simulations for
197 precipitation for the 0.44° and 0.11° CORDEX simulations respectively, with 15 in the common subset; 22 and 18
198 respectively for temperature, with 14 in the common subset. For wind, data was very limited for CORDEX at 0.44°
199 and there was no overlap of models with those used for the 0.11° simulations. Therefore, the wind analysis in the main
200 manuscript is based only on CORDEX 0.11° and CMIP5. There were 31 simulations for wind for CORDEX 0.11°,
201 with 15 in the common subset. CORDEX 0.11° and 0.44° were compared instead using the variable sfcWindmax (daily
202 maximum wind) which was available for 9 models at both resolutions (see Figure S8). There seemed to be
203 inconsistencies in the way sfcWindmax was calculated between CMIP5 models (mostly yielding stronger annual
204 maximum winds compared to using 3 hourly data to varying extents, but sometimes weaker), which precluded basing
205 the full analysis on this variable. When calculating ensemble medians for the common subset of simulations, we repeat
206 GCM members that drive more than one RCM. The number of CMIP5 simulations used for the extended ensemble
207 was 44 for precipitation, 42 for temperature and 25 for wind.

208

209 **2.2.2 UPSCALE simulations**

210 In order to examine the benefits or otherwise of differences in resolution for a global model, we make use of simulations
211 undertaken as part of the UPSCALE project (UK on PRACE: weather-resolving Simulations of Climate for globAL
212 Environmental risk; Mizieliński et al. 2014). This consists of the atmosphere only version of the Hadley Centre Global

213 Environment Model 3 (HadGEM3-A) run at three different resolutions: N96 (130 km), N216 (60 km) and N512 (25
214 km), all with 85 vertical levels for the period 1985-2011, with 5, 3 and 5 ensemble members respectively (or 3, 3 and
215 5 for wind data). The simulations are forced by observed records of greenhouse gases, aerosols, ozone, solar variability
216 and volcanic forcings following the AMIP-II procedure (Taylor et al. 2000), but using the higher resolution OSTIA
217 analysis (Operational Sea Surface Temperature and Sea Ice Analysis) for sea surface temperatures (SSTs) and sea ice
218 (Donlon et al. 2012). Very few parameters differ between the resolutions, enhancing the comparability of the three
219 ensembles. We use daily precipitation data, daily maximum temperatures and 3-hourly wind (subsampled to 6-hourly).

220 **2.3 Regridding**

221 In order to compare models of different resolutions with each other and with the observational datasets it was necessary
222 to regrid variables to a common grid. Using a high resolution grid for evaluation would preserve the finer spatial detail
223 and localised extremes for high resolution simulations, but is sometimes considered unfair for coarse resolution models
224 which cannot be expected to simulate the same intensities of extremes even for a perfect simulation due to spatial
225 smoothing effects. If processes are captured better at higher resolution, improvements should still be visible when
226 regridded to coarser resolution (Prien et al. 2016; Fantini et al. 2018). However, the finer spatial detail is an inherent
227 advantage of high resolution and smoothing this out will result in partial information loss. We use the 0.5° regular
228 longitude-latitude grid of E-OBS since it is in-between the resolution of the CORDEX models and CMIP5, and is
229 computationally feasible. Some of the benefits of higher resolution may be lost by doing this, putting our results on
230 the conservative side. Nevertheless, sensitivity tests showed that results for MESAN did not change perceptibly by
231 using a 0.5° grid compared to a 0.1° grid. We regrid the daily data, before the calculation of annual extreme indices.

232
233 The sensitivity of the results to the regridding technique was investigated for a number of models of different
234 resolutions and compared to results based on using the original grids (Figure S1). For the coarser resolution models
235 (e.g. HadCM3) results for precipitation extremes were particularly sensitive to the regridding technique, with much
236 weaker extremes for some techniques e.g. distance-weighted average remapping and bilinear interpolation, with
237 unrealistic artefacts in the spatial patterns for many methods. For high resolution models, the regridding technique did
238 not make much difference to the results, although conservative remapping tended to dampen extreme precipitation,
239 particularly for CORDEX 0.11. Overall the nearest neighbour method was chosen for precipitation for everything
240 except CORDEX 0.11 and MESAN since it gave results very close to using the original grid for all model resolutions,
241 preserving the amplitude of extremes, and also having minimal artefacts when plotting spatial patterns of precipitation
242 extremes. For going from high to lower resolution (e.g. 0.11° to 0.5°) nearest neighbour is less appropriate since
243 information from only a subset of grid cells is incorporated. Therefore, bicubic remapping was used for CORDEX 0.11
244 and MESAN, which also replicated results using the original grid very well (Figure S1). Wind and temperature results
245 were also somewhat sensitive to regridding technique, particularly for the coarser models. The above choices also
246 seemed appropriate for these variables (nearest neighbour in most cases, but bicubic for CORDEX 0.11, MESCAN,
247 ERA5 and DYNAD), both in terms of replicating return period results using the original grid, and retaining the blocky
248 nature of the low resolution simulations in the spatial patterns.

249 **3 Methods**

250 **3.1 Extremes Indices**

251 In order to examine extremes, we adopt indices based on the ETCCDI indices (Zhang et al. 2011). For precipitation
252 these are the annual maximum daily precipitation (Rx1day) and the annual maximum consecutive 5-day total
253 (Rx5day). For temperature we use the annual maximum daily maximum temperature (TXx) and the annual maximum
254 consecutive 5-day mean of daily maximum temperature (TXx5day). Rx1day and TXx5day are presented in the figures,
255 whilst the other indices are commented on in the text. For wind we use the annual maximum of daily maximum wind,
256 which we refer to as (WindXx). This is based on 6-hourly data. These are therefore much rarer extremes than those
257 based e.g. on the 95th or even 99th percentile which would happen on average 1 in 20 days and 1 in 100 days
258 respectively. One drawback is that this makes robust statistics more challenging.

259
260 In order to examine how well the climate models simulate extremes and the differences between different resolutions,
261 we first examine the spatial patterns of the climatological mean values of the indices and their biases with respect to
262 observational datasets. We then examine return period plots (see definitions below) for a number of regions for each
263 index, which highlights any differences in the shape of the tails of the distribution of the extremes. The regions used
264 are based on the PRUDENCE regions (Christenson and Christenson 2007) and the IPCC SREX regions (Seneviratne
265 et al. 2012) and are shown in Figure S2 and Table S2. A subset of representative regions are presented here, with some
266 comments about the others.

267 **3.2 Return periods**

268 In order to calculate regional return periods and return values we first sort the data into ascending order for each grid
269 cell. The return periods are calculated as N/k where N is the number of years of data, and k is the rank, with $k=1$ for
270 the largest value. Return periods are therefore the inverse of the probability of an event exceeding a given value (called
271 the “return value”). This is an empirical approach and has the limitation that return periods cannot exceed the number
272 of years of data used (e.g. 36 years). This is still the case even if an extremely unusual event occurs. Fitting a GEV
273 would allow estimates for higher return periods, but this would still be an extrapolation. The area weighted regional
274 average is made, for given return periods, over the associated return values. To avoid complications from missing data,
275 grid cells in E-OBS with more than 5 days of missing data in any year during the period examined were masked for
276 the whole period. Having one or more years missing would complicate the calculation of regional mean return periods
277 and values. Models and observational datasets are masked to have the same spatial coverage, which is land only. A
278 common time period across the models being examined and the observations they are being compared to is chosen to
279 allow comparability. For the CMIP5 and CORDEX analysis 1970-2005 is used for temperature and precipitation and
280 1979-2005 for wind. For the UPSCALE runs we use 1985-2011 for temperature, and 1989-2010 for precipitation to
281 allow comparisons with MESAN (1986-2011 is used for the analogue analysis, see below) and 1986-2011 for wind.

282
283 In order to allow the shapes of the return period curves to be compared more easily between different types of models
284 (i.e. CMIP5 and CORDEX at both resolutions), we first adjust each model to have the same climatological mean value

285 of the extreme index in question. This effectively shifts the curves up or down, but does not change their shape, which
286 is the focus of these figures. Without such a shift, curves are too spread out to be able to discern differences in shape.
287 Therefore we cannot comment on mean biases of the extremes indices based on the return plots, but these biases are
288 already shown and discussed based on map figures (see section 3.1). We implement this adjustment by subtracting the
289 difference between the model climatology of the index in question and the climatology of the reference observational
290 dataset for each model at a grid cell level. We use E-OBS as the reference for temperature and precipitation, and
291 MESCAN for wind. The additional observational datasets shown in the return period plots are also adjusted in the
292 same way. For the UPSCALE simulations, results can also be examined without the need to shift the curves to a
293 common mean value because the same version of the same model is used for a given resolution, meaning that curves
294 for individual simulations tend to cluster together instead of having large mean differences. In this way, differences in
295 biases with resolution are also seen in the return period plots. Nevertheless, we also present UPSCALE results with
296 the adjustment in Figure S10 for comparison.

297
298 Confidence intervals for the observational datasets are calculated using a bootstrapping method. If, for example, the
299 analysis period was 1970-2005 (i.e. 36 years), 1000 random samples of 36 years from this period are chosen from the
300 same dataset, allowing the same year to be chosen more than once per iteration. For each random sample, the chosen
301 values are sorted for each grid cell and a regional average is calculated as above, effectively yielding 1000 return period
302 curves per region. The 5th and 95th percentile of these values are then calculated to give the confidence intervals.

303

304 **4 Results**

305 **4.1 The benefits of regional high resolution: EURO-CORDEX versus CMIP5**

306 **4.1.1 Temperature extremes**

307 Figure 1 shows the spatial patterns of the climatological mean of TXx5day for the period 1970-2005 for E-OBS, and
308 the multi-model medians (MMM) of CMIP5, and CORDEX at both resolutions, along with their biases with respect
309 to E-OBS. The same general pattern can be seen in both E-OBS and the models, with hotter extremes in the south and
310 cooler extremes in the north and over the mountains. At higher resolution the colder warm extremes over the Alps and
311 Carpathians become more distinct. For the “common subset” the pattern of biases relative to E-OBS is similar for both
312 CMIP5 and CORDEX with cold biases in the North and West and hot biases in the South-East. However, the hot biases
313 over the mountains reduce with higher resolution since the model topography is higher. The cold bias over Scandinavia
314 is also larger in CORDEX than in CMIP5. Biases for CORDEX using the whole ensemble are similar to those for the
315 common subset. For CMIP5 the hot biases over the south-east, and over mountain ranges are stronger when using all
316 simulations compared to the subset. Findings for TXx are similar, but hotter (not shown).

317

318 To give an idea of the level of consistency of results between models, results for individual models are shown in Figure
319 S3. Although the CMIP5 models agree on the general spatial pattern of temperature extremes, their absolute

320 magnitudes vary considerably, although all are too hot over the Alps. There are also substantial differences between
321 results from different RCMs, including those driven by the same GCM, although the driving GCM does seem to affect
322 the overall magnitude of the temperature extremes. Biases of individual RCMs do not appear systematically smaller
323 than that of their driving GCM. Patterns are very similar for the same GCM-RCM chains at the both 12.5 and 50 km
324 resolutions. Results for different ensemble members of the same GCM or GCM-RCM chain are very consistent,
325 suggesting that the differences between models are not due to internal variability.

326
327 In order to assess any effect of resolution on the shape of the tails of the statistical distribution of temperature extremes,
328 Figure 2 (left column) shows return period against magnitude for TXx5day for CMIP5, CORDEX at both resolutions
329 and E-OBS (see Methods). Results are shown for Northern, Central and Southern Europe, and are representative of
330 results for the smaller PRUDENCE regions that fall within their boundaries. There is no obvious difference in the
331 shape of the tails between CMIP5 and CORDEX. Agreement with E-OBS is good for the multi model median, although
332 many individual ensemble members lie outside the range of the observational uncertainty.

333
334 In summary, shapes of return period curves for temperature extremes appear to be insensitive to dynamical
335 downscaling based on comparing CMIP5 to CORDEX at 0.11° and 0.44° , but biases are affected, for instance over
336 mountains where hot biases decrease with resolution.

337 **4.1.2 Precipitation extremes**

338 Now we consider precipitation extremes for CMIP5 compared to CORDEX. Figure 3 shows the climatological mean
339 of Rx1day for E-OBS and the MMMs of CMIP5 and CORDEX at both resolutions, and their differences with respect
340 to E-OBS. The heaviest annual maximum precipitation totals in E-OBS occur over the Alps and the western side of
341 coastal mountain ranges, including western Norway and north-eastern Spain. A similar spatial pattern of precipitation
342 distribution can be seen in the models, although totals are lower in CMIP5, and higher in CORDEX. CMIP5 is drier
343 than E-OBS over most of Europe, particularly over the areas of maximum observed precipitation (i.e. over or near
344 mountains), whilst CORDEX is generally wetter than observed, particularly in these same locations, and at higher
345 resolution. Results using the entire ensembles are very similar to using the common subset of simulations. Previous
346 studies suggest that E-OBS underestimates precipitation extremes since it is not corrected for gauge undercatch and
347 has a relatively low underlying station density (e.g. Prein and Gobiet 2017). Therefore, we also repeat results relative
348 to the MESAN reanalysis (Figure S4) for the shorter period 1989-2005. MESAN uses a particularly high density of
349 stations in France (see Data section). The climatology of Rx1day is wetter in MESAN than in E-OBS over most of
350 Europe, most noticeably over the Alps and surrounding areas. This leads to the dry bias in CMIP5 appearing bigger,
351 and the wet bias in CORDEX decreasing, although it is still present in the 0.11° simulations. Using regional-scale very
352 high resolution datasets could improve agreement with the 0.11° simulations, since they tend to give heavier
353 precipitation extremes (Prein and Gobiet 2017). Gauge undercatch will also contribute to the difference, particularly
354 for precipitation extremes associated with strong winds and in snow dominated regions

355

356 Figure S5 shows results for individual models. Again, whilst models agree on the general pattern of precipitation
357 extremes – i.e. wettest over mountains, there are considerable inter-model differences concerning the magnitude,
358 particularly over complex orography. A number of CMIP5 models have too light extremes everywhere, but all
359 underestimate precipitation extremes over mountainous regions to a greater or lesser extent. RCMs systematically
360 simulate heavier precipitation extremes compared to their driving GCMs, particularly over mountains, and these
361 extremes tend to become heavier when moving from 0.44° to 0.11° in most cases. Many of the RCMs have heavier
362 precipitation extremes than seen in E-OBS over much of Europe at 0.44°, although this difference may disappear if
363 compared to MESAN. This difference gets bigger at higher resolution and is largest over mountainous regions. The
364 spatial patterns seem to be very RCM dependent, with limited influence of biases in the driving GCM. Again results
365 are very consistent between ensemble members of the same models.

366
367 Figure 2 (middle column) shows return period curves for Rx1day for Northern, Central and Southern Europe. There is
368 a clear separation in the tails of the distribution according to resolution, with CMIP5 having the lightest tails, CORDEX
369 0.44 in the middle, and CORDEX 0.11 with the heaviest tails across all regions (including the smaller PRUDENCE
370 regions – not shown). Results using the common subset of models or the full ensembles are similar to each other. E-
371 OBS tends to lie between CMIP5 and CORDEX 0.44 for southern Europe, and closer to CORDEX 0.44 in central and
372 northern Europe. Using MESAN gives slightly heavier tails in all three regions, particularly in southern Europe (Figure
373 S6) and France where station density is highest (not shown), causing the best agreement to occur with CORDEX 0.44
374 everywhere. Results for Rx5day are similar, but with marginally less separation between the resolutions, whilst over
375 Northern and Central Europe the best agreement with E-OBS happens at a slightly higher resolution than for Rx1day
376 – i.e. either with CORDEX 0.44 or the lower end of the range of CORDEX 0.11 (not shown).

377
378 In summary, precipitation extremes are wetter and heavier tailed with higher resolution, especially over mountainous
379 regions. CMIP5 has a dry bias, particularly over mountains, whilst CORDEX tends to be too wet relative to E-OBS,
380 particularly at 0.11°, but results are sensitive to observational dataset used, with wet biases for CORDEX reducing
381 when compared to the higher resolution MESAN dataset.

382 4.1.3 Wind Extremes

383 Finally, we examine annual maximum wind (WindXx). Figure 4 shows the multi model medians of climatological
384 mean annual maximum wind for CMIP5 and CORDEX at 0.11° compared to three reanalysis datasets. Data for
385 CORDEX 0.44° were very limited and did not overlap with the models used at 0.11° and so are not shown. The
386 MESCAN and DYNAD reanalyses show strong extreme winds over the UK, the Norwegian mountains and the NW
387 coastline of France through to Denmark. Relatively strong winds are also seen over the Spanish plateau, and a belt of
388 strong winds running zonally across central Europe between somewhat slower winds to the North and South. The
389 datasets differ in the magnitude of the winds, with DYNAD having more contrast between areas of low and high wind.
390 MESCAN should be the more accurate of the two (Tomas Landelius, personal communication). ERA5 has notably
391 slower winds, particularly over mountainous regions, but a similar overall zonal tripole pattern can be seen. Niemann

392 et al (2017) found that MESCAN underestimates extreme winds compared to station data over Germany. ERA5 must
393 therefore underestimate even more. Concerning mean winds, Jourdier (2020) find that ERA5 underestimates wind
394 speed compared to French stations, particularly over mountains.

395
396 The CMIP5 driving model median shows a similar overall pattern of WindXx as the reanalyses, particularly ERA5,
397 with a pattern of weaker winds in the north and south, and a belt of stronger winds in the middle. However, CMIP5
398 does not tend to have stronger winds over mountains like in DYNAD and MESCAN. Using the whole CMIP5 ensemble
399 gives similar results. The CORDEX multi model medians show generally higher wind speeds than CMIP5, and
400 captures the high wind speeds along western coastlines and over some mountainous terrain. Results for the common
401 subset of simulations are similar to those obtained from the complete CORDEX ensembles, except that the latter shows
402 slow wind speeds over the Alps instead of high. This latter feature is very RCM dependent, and indeed the overall
403 pattern and magnitude of the extreme winds almost entirely reflects the choice of RCM with very little influence of
404 GCM (Figure S7). For some RCMs the zonal tripole pattern is the clearest feature (ALADIN, COSMOcrCLIM), whilst
405 for others it is the high winds over mountains and coastlines (RCA, HIRHAM5). The driving GCMs differ considerably
406 in terms of the magnitude of extreme winds, but have a similar overall pattern to each other (Figure S7). Ensemble
407 members of the same model give very similar results for both CORDEX and CMIP5. Multi-model median biases are
408 dependent on the reanalysis used for reference, with CORDEX 0.11 being close to DYNAD, and CMIP5 being closest
409 to ERA5. In order to compare the two resolutions of CORDEX, results based on sfcWindmax instead of 3 hourly wind
410 are presented in Figure S8 (see methods). Winds are either similar between the two resolutions (e.g. RCA and WRF),
411 or stronger at higher resolution (RACMO, HIRHAM5). Again the overall pattern is very RCM dependent.

412
413 Figure 2 (right column) shows return period plots for WindXx for CMIP5 and CORDEX at 0.11°. The British Isles
414 are shown instead of Northern Europe, since they are particularly affected by wind extremes, and for comparison with
415 the results for the UPSCALE simulations, where this region shows distinctive results. The distribution of annual
416 maximum sfcWindmax has somewhat heavier tails in CORDEX 0.11 compared to CMIP5, regardless of the subset of
417 models used in calculating the multi-model median in all regions examined. CORDEX 0.11 tends to be closest to
418 DYNAD and MESCAN, whilst CMIP5 is closest to ERA5. Figure S9 shows that when using sfcWindmax, CORDEX
419 0.11 has heavier tails than CORDEX 0.44.

420
421 In summary, winds tend to be somewhat stronger, with somewhat heavier tails at higher resolution, with a large spread
422 between models. Reanalysis datasets give fairly diverse results.

423
424 **4.2 Global high resolution: UPSCALE**

425 We now examine the benefits or otherwise of global high vs. standard resolution simulations for simulating climate
426 extremes. Global high resolution may allow an improved representation of the large scale circulation that cannot be
427 captured by regional models, which may in turn affect the representation of climate extremes. For this we examine the

428 UPSCALE simulations (Mizielinski et al. 2014), which consist of a small ensemble of HadGEM3-A simulations at
429 three different resolutions: 130km (N96), 60km (N216), and 25km (N512) (see Data section).

430 **4.2.1 Temperature extremes**

431 Figure 5 shows the ensemble mean climatological mean of TXx5day for the UPSCALE simulations over the period
432 1985-2011 at all three resolutions, and their biases relative to E-OBS. The same general pattern of hotter extremes in
433 the south and colder in the north and over mountainous regions can be seen at all three resolutions, but temperature
434 extremes are hotter at higher resolution in the south and east, and colder over mountains. The same pattern of biases is
435 seen as for CORDEX and CMIP5 with cold biases in the north and hot in the south-east and over mountains. The
436 mountain biases reduce with higher resolution, as the orography becomes better defined, whilst the hot bias in the SE
437 and SW increases and the northern cold bias improves slightly. A coastal cold bias at low resolution disappears at
438 higher resolution as the model land mask becomes more detailed. Note that the SSTs are prescribed and are the same
439 for all simulations. Results for TXx are similar but hotter (not shown).

440
441 Figure 6 (left column) shows regional return period plots for TXx5day for the UPSCALE simulations. Results are a
442 little less consistent across regions for UPSCALE compared to the CMIP5 vs CORDEX analysis, so we split Northern
443 Europe into the British Isles and Scandinavia, and add the Alps, to better capture regional variations. Since the
444 ensemble means are only based on one model, results are presented without adjusting according to the climatology of
445 TXx5day, although such adjusted results can be seen in Figure S10 and allow differences in the shapes of the tails to
446 be seen more clearly. TXx5day seems to be somewhat hotter with higher resolution over many regions, although this
447 is not always clear cut. The Alps are a notable exception, where the higher elevations with higher resolution give rise
448 to colder temperature extremes. There are notable biases relative to E-OBS, with the models being too cold in the
449 north, especially at low resolution, whilst in the south the colder subset of models (N96, the lowest UPSCALE
450 resolution) agree best with the E-OBS. Over the Alps, again the low resolution simulations agree best with E-OBS,
451 with the warmest temperatures, but this will depend on the height of the meteorological stations. This apparent
452 contradiction to the reduced orographic hot bias with resolution in Figure 5 comes from the stronger cold bias of the
453 surrounding areas at low resolution. Figure S10 shows that differences between the shape of the tails with resolution
454 are not systematic across regions and are mostly small, whilst agreement with E-OBS is good everywhere. Results for
455 TXx are similar.

456
457 In summary, hot biases of temperature extremes over mountains reduce with increased resolution for HadGEM3-A.
458 Elsewhere extremes tend towards getting hotter with resolution, whilst the shapes of the return period curves are
459 insensitive.

460 **4.2.2 Precipitation extremes**

461 For precipitation, Figure 7 shows the ensemble mean climatological mean of Rx1day for the period 1989-2010 for the
462 three UPSCALE ensembles and their differences relative to E-OBS and MESAN. The overall pattern of Rx1day in the

463 simulations is similar to that in the observational datasets, with heavier precipitation extremes and finer spatial detail
464 with increasing resolution over complex orography. All resolutions have bands of heavy precipitation either side of
465 the Alps, but these move closer together as the Alps become better defined. All simulations are generally wetter than
466 E-OBS across most of Europe. The dry bias over orography in the Alps, Southern Norway and Scottish Highlands
467 reduces with resolution, whilst a wet bias on the southern edge of the Alps and the coastal side of the Dinaric Alps in
468 the Balkans appears instead. Comparing to MESAN instead of E-OBS, the general wet bias disappears, and the dry
469 mountain bias over orography at low resolution increases. The differences between resolutions appear smaller than for
470 the CMIP5 versus CORDEX analysis: all the UPSCALE simulations look most similar to CORDEX at 0.44°.
471 However, UPSCALE does not reach as fine a resolution as CORDEX at 0.11° (25 km vs 12.5 km), and CMIP5 is on
472 average slightly coarser than the N96 simulations. In addition, it should be noted that models with the same nominal
473 resolution do not necessarily have the same effective resolution, and that the effective resolution is always less than
474 the nominal resolution (Skamarock 2004; Klavar et al. 2020). Results are similar for Rx5day (not shown).

475
476 Figure 6 (middle column) shows the return period plots for Rx1day for the three resolutions of UPSCALE ensembles.
477 Slightly heavier precipitation extremes are found at higher resolution in all the regions shown (exceptions are France
478 and Mid Europe- not shown). Although the differences are small, they are more obvious in southern Europe and
479 especially in the Alps. Figure S10 shows that there is not much difference in the shape of the tails for most regions,
480 although there are very slightly heavier tails at higher resolution for southern Europe (more so in the Mediterranean
481 sub region- not shown) and more obvious differences over the Alps in the same direction, both of which are regions
482 where convective precipitation is important. E-OBS tends to lie just below the model simulations for most regions
483 (Figure 6), although it agrees with the models for the British Isles, and is between the low and medium resolution
484 simulations over the Alps. MESAN gives higher values for observed Rx1day which improves agreement in regions
485 where E-OBS lay below the models, and causes a higher resolution subset to agree better in the other regions (Figure
486 6). For the curves that are adjusted to have the same climatological mean, E-OBS tends to lie just on the lower end of
487 the ensemble for most regions, whilst MESAN gives slightly heavier tails and tends to improve agreement with models
488 (Figure S10). Results for Rx5day are broadly similar (except that both observational datasets lie above all the models
489 for the British Isles).

490
491 In summary, precipitation extremes are somewhat wetter and heavier tailed with increasing resolution mostly in
492 southern Europe and the Alps for HadGEM3-A. Dry orographic biases decrease with resolution, but wet biases appear
493 in the south next to mountain ranges instead.

494 **4.2.3 Wind extremes**

495 For wind extremes, Figure 8 shows the spatial patterns of climatological mean annual maximum wind for UPSCALE
496 and the same for three reanalyses. The spatial patterns are similar for the three different model resolutions, with the
497 highest winds over the British Isles and coastal regions, lower wind speeds over the Alps, and the zonal tripole pattern
498 described above. The main differences are that the lower resolution model (N96) has stronger winds around the British

499 Isles and western coastlines. This is likely because the larger coastal grid boxes overlap more with the ocean, which
500 tends to have higher wind speeds, or due to differences in the model land mask itself with resolution. The wind speeds
501 at higher resolution are a little stronger overall, most obviously in the central European zonal belt, and over the Alps
502 and Norwegian mountains. All resolutions show stronger winds than ERA5 over most of Europe. Compared to
503 MESCAN winds are too weak in the northern and southern Europe, particularly over mountainous regions, and a little
504 too strong in between. Relative to DYNAD the pattern of differences is similar as for MESCAN, but with stronger
505 negative differences over the Norwegian mountains and positive differences in other parts of Northern Europe. There
506 are positive coastal biases relative to all reanalyses for the N96 simulations that reduce with increased resolution.

507
508
509 Figure 6 (right column) shows the return period plots for some example regions for annual maximum wind for the
510 UPSCALE simulations, without shifting the climatology. Over all regions examined (except the Mediterranean- not
511 shown), the N512 simulations have stronger winds than the N216 simulations. The position of the curve for N96 is
512 strongly related to how much coastline there is relative to land area per region, e.g. with faster winds than the other
513 simulations over the British Isles and southern Europe, but relatively slower winds over central Europe, and particularly
514 over the Alps. There are fairly large differences between reanalysis estimates, with ERA5 always having the slowest
515 winds, and the model simulations tending to lie between ERA5 and the other two reanalyses for most regions. For the
516 adjusted versions of the return period plots (Figure S10), differences in the shapes of the tails with resolution are
517 generally small, although with marginally heavier tails with increasing resolution over a number of regions, e.g the
518 Alps (not all are shown). MESCAN and DYNAD have slightly heavier tails than ERA5, particularly over the Alps and
519 Southern Europe. The shape of the model curves agree well with all reanalyses over the British Isles, Scandinavia and
520 Central Europe, and lie between ERA5 and the other two reanalyses for the Alps and Southern Europe.

521
522 In summary winds are slightly stronger and heavier tailed at higher resolution in HadGEM3-A, except over coastal
523 areas where large coastal grid boxes at low resolution bring strong ocean winds further over land.

524 **4.3 Upscaling versus downscaling**

525 For the global model results, any differences in the representation of extremes according to resolution could come from
526 either upscaling or downscaling effects. Upscaling effects could include a better representation of the large scale
527 circulation, whilst downscaling allows a better representation of small scale processes, such as convection, and an
528 improved representation of orography and coastlines. In order to investigate which of these effects leads to the
529 differences between the low (N96) and high resolution (N512) HadGEM3-A simulations, we employ a circulation
530 analogue technique (e.g. Vautard et al., 2016), which is frequently used in attribution studies (see e.g. Stott et al., 2016;
531 Cattiaux et al., 2010). The idea is to determine whether the simulation of climate extremes changes between the two
532 resolutions if both were to have the same large scale circulation –i.e. isolating the downscaling effect, or conversely
533 whether circulation differences explain any differences in extreme events whilst circulation-variable (e.g. precipitation)
534 relationships stay the same –i.e. the upscaling effect.

535
536 For each day in the lower resolution simulations we pick the nearest circulation analogue from anywhere in the higher
537 resolution simulations, providing it happens at the right time of year (i.e. within a 30-day window centred on the day
538 of the year in question). We then record the associated temperature, precipitation and wind values from the higher
539 resolution simulations to make a “*u*-chronic” dataset (e.g. Jézéquel, et al. 2018) that contains data from the high
540 resolution simulations but follows the daily sequence of circulation patterns from the low resolution models. We then
541 repeat the analysis of return periods and value as above. We also do the reverse (find analogues for the N512 circulation
542 in the N96 ensemble and record the N96 temperature). Since results using analogues are not directly comparable to the
543 original results due to the lack of an exact analogue match, we also perform “self-analogues” -i.e. finding circulation
544 analogues for the N96 simulations within the N96 ensemble, (excluding the same year from the same ensemble
545 member) and creating a *u*-chronic time series, and the same for the N512 ensemble). Comparing the resulting return
546 period curves tells us about the contribution of large-scale circulation and downscaling to differences in extremes
547 between the two resolutions. For example, comparing the N96 self-analogue return curve to the version based on N512
548 circulation but with N96 precipitation shows us the contribution of any differences in the large scale circulation
549 between the resolutions i.e. the upscaling effect. Comparing the N96 self-analogue to the version based on N96
550 circulation with N512 precipitation shows us the downscaling effect – i.e. any difference between the relationship
551 between the large scale circulation and precipitation.

552
553 Analogues are defined using geopotential height at 500 hPa, since this avoids complications relating to surface heat
554 lows associated with heat waves in anticyclonic conditions that occur in summer, whilst also avoiding incomplete data
555 due to mountain ranges. Geopotential height is regridded to a 2° grid using bilinear interpolation. This choice ensures
556 that we are comparing analogues with the same resolution and do not penalise small-scale differences. Similarity
557 between circulation states is quantified using pattern correlation, which is not affected by trends in geopotential height
558 with global warming. For precipitation and wind the European domain used is -16 to 44° E and 34 to 72° N (roughly
559 the same as the domain plotted in the map-based figures). For temperature, a larger domain is used, since the history
560 and trajectory of air masses are important for temperature extremes. This domain is loosely based on the domain used
561 by Cattiaux et al. (2010) and extends over the N. Atlantic as well as Europe, (-62 to 44°E and 24 to 80° N). However,
562 results are very similar if the smaller domain is used (not shown). For the 5-day variables (Rx5day and TXx5day) the
563 *u*-chronic dataset was smoothed using a 5-day running mean at the end of the process. We also tried smoothing the
564 daily geopotential height, precipitation and temperature datasets first and then performing the analogue analysis. The
565 relationship between the different curves was largely consistent between the two techniques, but absolute values
566 differed and the shape of the curves changed a little. Results presented here are based on the first technique.

567
568 Figure 9 shows the results of the analogue analysis. The blue curves show the results for the N512 self-analogues, grey
569 represents the N96 self-analogues, red represents results using the circulation patterns from the N96 runs but with the
570 N512 circulation-variable relationships, and green indicates N512 circulation with N96 circulation-variable
571 relationships. The difference between the blue and red curves (or the grey and green curves) shows the contribution

572 from differences in the large scale circulation with resolution, whilst the difference between the blue and green curves
573 (or the red and grey curves) indicates the downscaling effect.

574
575 For TXx5day downscaling effects are dominant over regions that have a clear difference between resolutions, although
576 circulation differences also have a small effect in some regions such as the British Isles (Figure 9). For Rx1day the
577 different curves are very close together for some regions, making it difficult to discern the relative contributions from
578 upscaling and downscaling. However, for regions with an obvious difference between resolutions, such as the Alps
579 and Southern Europe, it seems to be downscaling effects that are the most important. Interestingly, these are regions
580 where convective precipitation is particularly important for precipitation extremes. For wind extremes downscaling
581 effects also dominate, particularly over the British Isles, central Europe and the Alps. Results for TXx and Rx5day are
582 very similar to those for TXx5day and Rx1day respectively (not shown).

583
584 Also shown, using dashed lines, are the original ensemble mean results without using analogues. By comparing these
585 with the self-analogue results we can see how successful the analogue technique is in recreating the original
586 distributions. The self-analogue results tend to be close to the original results for wind and Rx1day, but below them
587 for Tx5day. Undertaking the 5-day averaging first rather than last (see above) shifts analogue results upwards, above
588 the original curves, but the other aspects of the results are the same (not shown). A similar phenomenon is seen for
589 Rx5day (not shown).

590
591 In summary, for all three types of extreme events, downscaling effects appear to dominate the differences seen between
592 the 130km and 25km HadGEM3-A simulations. This suggests that at least for this model, any large scale circulation
593 differences obtained with global high resolution do not affect the statistics of these extreme events much.

594 **5 Discussion and Conclusions**

595 We evaluated climate model simulations of temperature, precipitation and wind extremes over Europe, addressing
596 three questions: 1) The benefits of dynamical downscaling using regional climate models by comparing EURO-
597 CORDEX simulations at two resolutions (12.5 and 50 km) to their driving coarser resolution CMIP5 models; 2) The
598 benefits of increased resolution for global models by comparing HadGEM3-A simulations at three resolutions (130,
599 60 and 25 km; referred to as the “UPSCALE” simulations); and 3) whether any differences according to resolution in
600 the global model comes from differences in the large scale circulation (upscaling) or the representation of small scale
601 processes, and features (downscaling) using a circulation analogue method.

602
603 For temperature extremes, increased resolution did not make much difference to results for the CORDEX vs CMIP5
604 analysis in terms of the shapes of the return period curves, which all agreed well with observational data. Hot biases
605 over mountains reduced with increased resolution, although the cold bias over Scandinavia was worse in CORDEX
606 than in CMIP5. This amplified Scandinavian cold bias in CORDEX is consistent with the findings of Sørland et al
607 (2018) for mean summer temperature, although we did not find the same reduction of the warm bias in Eastern Europe

608 in CORDEX as they did, possibly due to differences in the models used. Our findings agree with Vautard et al. (2013),
609 who find limited benefits in simulating various aspects of heatwaves between the 0.44° and 0.11° versions of the
610 EURO-CORDEX models. The reduction in orographic bias with increased resolution was also seen in the HadGEM3-
611 A GCM simulations, along with a general tendency towards hotter extremes elsewhere, which reduces biases in the
612 north, and increases them in the south. Overall the benefits of increasing resolution were limited, or region dependent.
613 However, our results for the global model analysis are based on only one model and the new model simulations and
614 analyses being generated as part of the PRIMAVERA and HighResMIP projects (<https://www.primavera-h2020.eu/>;
615 Roberts et al. 2018; Haarsma et al. 2016) will be very useful for determining how representative our results for
616 HadGEM3-A are of other GCMs. For instance, improvements in the simulation of summer blocking, which can be
617 involved in heatwave generation is very model dependent (Scheimann et al. 2014). Furthermore, Cattiaux et al. (2013)
618 find that the frequency, intensity and duration of summer heatwaves improve in the IPSL model with resolution,
619 associated with a better representation of the large scale circulation. In addition, here we examine only one aspect of
620 heat waves (intensity), and it could be that results are different for other aspects, such as frequency, duration and
621 timing.

622
623 Precipitation extremes were more sensitive to resolution, particularly in the CMIP5 vs CORDEX analysis, with heavier
624 tails at higher resolution across all regions. Spatially, CMIP5 shows a general dry bias compared to E-OBS, particularly
625 over mountainous regions, whilst CORDEX shows the opposite, with increasing wet differences at 0.11° compared to
626 0.44°, which appears to be systematic across models. This is consistent with results for mean precipitation in EURO-
627 CORDEX in Kotlarski et al. (2014). The higher resolution MESAN reanalysis gave wetter extremes and heavier tails
628 than E-OBS, agreeing best with the 0.44° resolution CORDEX simulations. Other studies suggest that country-scale
629 higher resolution precipitation datasets give heavier precipitation extremes still, which may agree best with the 0.11°
630 simulations. Similarly, for mean precipitation, Prein and Gobeit (2017) find that RCM biases are a similar size to the
631 differences between different observational estimates. For extreme precipitation, various studies find that a number of
632 aspects (biases, frequency-intensity distributions, spatial patterns) of mean and extreme precipitation improve in
633 EURO-CORDEX at 0.11° compared to 0.44° when compared to such high resolution datasets (e.g. Prein et al. 2016;
634 Torma et al. 2015; Fantini et al. 2020). Prein et al (2016) ascribe this mostly to the better representation of orography
635 at higher resolution, but also the ability to capture the larger scales of convection. However, aside from improved
636 spatial patterns Casanueva et al (2016) found only limited evidence for improvements in precipitation intensity,
637 frequency and derived indicators over the Alps and Spain with resolution in EURO-CORDEX. Some of the differences
638 with resolution in our results may also be explained by parameterisation schemes that tend to be tuned to one resolution
639 and can behave sub-optimally at others.

640
641 For the UPSCALE global simulations, there was less difference in extreme precipitation with resolution, with the
642 biggest differences in southern regions or over or near mountains, with heavier tails and wetter extremes at higher
643 resolution. This reduced dry biases over orography, but wet biases next to some mountain ranges in the south emerged
644 instead. However, these simulations span a narrower range of resolutions, i.e. not reaching the same high resolutions
645 as CORDEX 0.11°, but also not as coarse as some CMIP5 models. Other global model studies also tend to find an

646 increase in precipitation extremes with increased resolution for Europe, which is continent-wide in summer, and
647 concentrated in mountainous regions in winter (Volosciuk et al. 2015; Wehner et al. 2014). This sometimes improves
648 agreement with observational data (e.g. Kopparla et al. 2013; Wehner et al. 2014 for winter), but can overestimate
649 summer extreme precipitation if parameterisation schemes are not retuned (Wehner et al. 2014).

650
651 For wind extremes, higher resolution gave somewhat stronger winds and heavier tails for most regions for both the
652 CORDEX vs CMIP5 analysis and to a lesser extent for HadGEM3-A, except for regions dominated by coasts for the
653 latter, where large coastal grid boxes at lower resolution brought strong ocean winds further over land. Stronger winds
654 with higher resolution are also found in previous studies (e.g. Pryor et al. 2012; Kunz et al. 2010; Gao et al. 2020). The
655 largest differences we found were between CMIP5 and CORDEX at 0.44°, with less difference between the two
656 resolutions of CORDEX. Differences between reanalysis based estimates made model evaluation difficult.

657
658 The results of the circulation analogue analysis on the HadGEM3-A GCM simulations suggested that downscaling
659 effects were the dominant cause of differences with resolution for all three phenomena, with limited effects of any
660 differences in the representation of the large scale circulation. If this result also applied to other GCMs, it would suggest
661 that dynamical downscaling with more economical limited area models would be a better strategy for simulating
662 European extreme events, whilst GCM efforts could focus on other aspects such as multiple members or multi-physics
663 ensembles. However, we cannot reach this conclusion based solely on this analysis, since we examine only a single
664 model, which may not be representative of other models, and because the range of resolutions considered may be too
665 narrow. Demory et al. (2020) and Strandberg and Lind (2020) found that PRIMAVERA GCM simulations and EURO-
666 CORDEX simulations at comparable resolution simulated fairly similar precipitation PDFs to each other, which would
667 agree with a limited influence of upscaling. However, a number of studies do find improvements in the large-scale
668 circulation with resolution, including for extra-tropical cyclones and storm tracks (Colle et al. 2013; Jung et al 2006;
669 2012, Zappa et al. 2013), Euro-Atlantic weather regimes (Dawson et al. 2012; 2015; Cattiaux et al. 2013; Strommen
670 et al. 2019; Fabiano et al. 2020) and blocking (Jung et al. 2012, Anstey et al. 2013; Matsueda et al. 2009, Berckmans
671 et al 2013; Scheimann et al. 2017; 2020; Davini et al 2017a; 2017b; 2020; see also Introduction). Interestingly,
672 Scheimann et al. (2017) find improvements in Euro-Atlantic blocking with resolution in all seasons in the same
673 HadGEM3-A simulations as we analyse here. However, the net effects on extremes, given all uncertainties, was not
674 explicitly investigated. Our study does not seem to be able to discern such effects. Other studies suggest that benefits
675 from upscaling may require convective permitting simulations (Hart et al. 2018).

676
677 Overall our results suggest that whether or not increased resolution is beneficial for the simulation of extreme events
678 over Europe depends on the event being considered. Benefits appear limited for heatwaves, whereas wind extremes
679 and particularly precipitation extremes are more sensitive. We do not find any particular advantage in using a global
680 high resolution model compared to regional dynamical downscaling, with the caveats that this investigation needs to
681 be extended to other GCMs, and a wider range of resolutions should be investigated.

682

683 In order to fully address the question of the benefits of increased resolution for European climate extremes, a number
684 of aspects remain to be investigated. Firstly, the analysis could be widened to other types of extremes, for example,
685 sea level rise and storm surge, or other aspects of extremes could be considered e.g. timing, frequency and duration of
686 events. The global simulations we investigated were atmosphere-only, and the role of increased ocean resolution and
687 also vertical resolution and model top height should be considered. Finally, we assume that better historical
688 performance translates into more accurate future projections. Lhotka et al. (2018) find low sensitivity of heatwave
689 projections to resolution in EURO-CORDEX RCMs. However, Van Haren et al. (2015b) and van der Linden et al.
690 (2019) find stronger future summer drying and heating in central Europe with increased resolution in the EC-Earth
691 GCM due to differences in atmospheric circulation. Concerning precipitation, future projections for large scale and
692 seasonal mean precipitation are consistent between large scale regional and convective permitting models, whilst there
693 is evidence that summer sub-daily intensities increase more in the future in convection permitting models (Kendon et
694 al. 2014; 2017; Ban et al. 2015). For wind, Willison et al. (2015) find a larger response of the North Atlantic storm
695 track to global warming with higher resolution in the regional WRF model. Furthermore, Baker et al. (2019) find that
696 in winter the polar jet, storm tracks and associated precipitation shift further North over the Euro-Atlantic region in the
697 future with increased resolution in the same HadGEM3-A set up as used here. The sensitivity of projections to
698 resolution nevertheless remains an area that needs further research.

699
700 Finally, ongoing projects such as HighResMIP for CMIP6 (Haarsma et al., 2016), and the CORDEX Flagship Pilot
701 Studies, particularly the FPS on Convective Phenomena at High Resolution over Europe and the Mediterranean
702 (Coppola et al., 2019; Jacob et al 2020), will enable the benefits of high resolution and its effect on European climate
703 projections to be explored more thoroughly. The former will allow a systematic exploration of the effects of increased
704 resolution for multiple GCMs through coordinated experiments simulating the past and future climate. The latter will
705 include a first of its kind large multi-model ensemble at convective permitting resolution for decadal time slices in the
706 present and future for a large domain covering central Europe and part of the Mediterranean.

707 **Data and code availability**

708 The CMIP5 and CORDEX data used for this analysis are available from the Earth System Grid Federation portals, and
709 are detailed in Table S1. The HadGEM3-A UPSCALE simulations are available from the CEDA-JASMIN platform.
710 E-OBS can be downloaded here <https://www.ecad.eu/download/ensembles/download.php>, MESAN is available here
711 <http://exporter.nsc.liu.se/620eed0cb2c74c859f7d6db81742e114/>, ERA5 and MESCAN are available from the
712 Copernicus Climate Data Store <https://cds.climate.copernicus.eu>, whilst DYNAD winds are available from Tomas
713 Landelius at SMHI.

714 **Author contributions**

715 CI, RV and SJ conceptualised the study, CI carried out the analysis and wrote the manuscript, JS managed the CRECP
716 project together with CH and BE, and all co-authors were involved in discussions to prepare the study and helped
717 improve the manuscript.

718 **Competing interests**

719 The authors declare that they have no conflict of interest.

720 **Acknowledgements**

721 This work is published in the name of the European Commission, with funding from the European Union through the
722 Copernicus Climate Change Service project C3S_34a Lot 3 (Copernicus Roadmap for European Climate Projections).
723 The Commission is not responsible for any use that may be made of the information contained. We acknowledge the
724 WCRP's Working Group on Regional Climate, and the Working Group on Coupled Modelling - the coordinating body
725 of CORDEX and the panel responsible for CMIP5 respectively. We thank the climate modelling groups for producing
726 and making available the model output listed in Supplementary Table 1, which is available at <http://pcmdi9.llnl.gov>.
727 For CMIP, the US Department of Energy's Program for Climate Model Diagnosis and Intercomparison provides
728 coordinating support and led development of software infrastructure in partnership with the Global Organization for
729 Earth System Science Portals. We thank the modelling team that produced the UPSCALE simulations, and
730 acknowledge the JASMIN and IPSL mesocentre computing clusters on which this analysis was performed. We thank
731 Tomas Landelius from SMHI for making the DYNAD wind data available. We also acknowledge helpful input from
732 the CRECP project scientific advisory board and useful discussions with UK Met Office Scientists, in particular
733 Malcolm Roberts and Carol McSweeney.

734

735 **References**

736 Anstey, J. A., Davini, P., Gray, L. J., Woollings, T. J., Butchart, N., Cagnazzo, C., Christiansen, B., Hardiman, S. C.,
737 Osprey, S. M. and Yang, S.: Multi-model analysis of Northern Hemisphere winter blocking: Model biases and the role
738 of resolution, *J. Geophys. Res. Atmos.*, 118, 3956–3971, doi: 10.1002/jgrd.50231, 2013.

739

740 Bador, M., Boé, J., Terray, L., Alexander, L. V., Baker, A., Bellucci, A., Haarsma, R., Koenigk, T., Moine, M-P.,
741 Lohmann, K., Putrasahan, D. A., Roberts, C., Roberts, M., Scoccimarro, E., Schiemann, R., Seddon, J., Senan, R.,
742 Valcke, S., and Vanniere, B.: Impact of higher spatial atmospheric resolution on precipitation extremes over land in
743 global climate models. *J. Geophys. Res. Atmos.*, 125, e2019JD032184. <https://doi.org/10.1029/2019JD032184>, 2020

744

745 Baker, A.J., Schiemann, R., Hodges, K. I., Demory, M., Mizielinski, M. S., Roberts, M. J., Shaffrey, L. C., Strachan,
746 J. and Vidale, P. L.: Enhanced Climate Change Response of Wintertime North Atlantic Circulation, Cyclonic Activity,
747 and Precipitation in a 25-km-Resolution Global Atmospheric Model. *J. Climate*, 32, 7763–7781, [https://doi-
748 org.ezproxy.is.ed.ac.uk/10.1175/JCLI-D-19-0054.1](https://doi-org.ezproxy.is.ed.ac.uk/10.1175/JCLI-D-19-0054.1), 2019

749

750 Ban, N., Schmidli, J. and Schär, C.: Heavy precipitation in a changing climate: Does short-term summer precipitation
751 increase faster?, *Geophys. Res. Lett.*, 42, 1165–1172, doi: 10.1002/2014GL062588, 2015.

752

753 Bazile, E., Abida, R., Verrelle, A., Le Moigne, P. and Szczypta, C. : Report for the 55years MESCAN-SURFEX re-
754 analysis, deliverable D2.8of the UERRA project, pp. 22, available from: [http://www.uerra.eu/publications/deliverable-
756 reports.html](http://www.uerra.eu/publications/deliverable-
755 reports.html), 2017

757 Berckmans, J., Woollings, T., Demory, M. E., Vidale, P.-L. and Roberts, M.: Atmospheric blocking in a high resolution
758 climate model: influences of mean state, orography and eddy forcing, *Atmos. Sci. Lett.*, 14, 34–40,
759 doi:10.1002/asl2.412, 2013.

760 Casanueva, A., Kotlarski, S., Herrera, S., Fernández, J., Gutiérrez, J.M., Boberg, F., Colette, A., Christensen, O. B.,
761 Goergen, K., Jacob, D., Keuler, K., Nikulin, G., Teichmann C. and Vautard, R.: Daily precipitation statistics in a
762 EURO-CORDEX RCM ensemble: added value of raw and bias-corrected high-resolution simulations, *Clim Dynam*,
763 47,719-737. <https://doi.org/10.1007/s00382-015-2865-x>, 2016

764

765 Cattiaux, J., Vautard, R., Cassou, C., Yiou, P., Masson-Delmotte, V., and Codron, F.: Winter 2010 in Europe: A cold
766 extreme in a warming climate, *Geophys. Res. Lett*, 37, L20704, doi: 10.1029/2010GL044613, 2010.

767

768 Cattiaux, J., Quesada, B., Arakélian, A., Codron, F., Vautard, R., Yiou, P.: North-Atlantic dynamics and European
769 temperature extremes in the IPSL model: sensitivity to atmospheric resolution, *Clim. Dynam.*, 40, 2293-2310,
770 doi:10.1007/s00382-012-1529-3, 2013.

771

772 Christensen, J. H. and Christensen, O. B.: A summary of the PRUDENCE model projections of changes in European
773 climate by the end of this century, *Climatic Change*, 81, 7–30, doi: 10.1007/s10584-006-9210-7, 2007.

774

775 Colle, B. A., Zhang, Z., Lombardo, K., Liu, P., Chang, E. and Zhang, M.: Historical evaluation and future prediction
776 in Eastern North America and western Atlantic extratropical cyclones in the CMIP5 models during the cool season, *J.
777 Climate.*, 26, 882–903, doi: 10.1175/JCLI-D-12-00498.1, 2013.

778

779 Coppola, E., Sobolowski, S., Pichelli, E., Raffaele, F., Ahrens, B., Anders, I., Ban, N., Bastin, S., Belda, M., Belusic,
780 D., Caldas-Alvarez, A., Margarida Cardos, R., Davolio, S., Dobler, A., Fernandez, J., Fita Borrell, L., Fumiere, Q.,
781 Giorgi, F., Goergen, K., Guettler, I., Halenka, T., Heinzeller, D., Hodnebrog, Ø., Jacob, D., Kartsios, S., Katragko, E.,

782 Kendon, E., Khodayar, S., Kunstmann, H., Knist, S., Lavín, A., Lind, P., Lorenz, T., Maraun, D., Marelle, L., van
783 Meijgaard, E., Milovac, J., Myhre, G., Panitz, H.-J., Piazza, M., Raffa, M., Raub, T., Rockel, B., Schär, C., Sieck, K.,
784 Soares, P. M. M., Somot, S., Srncic, L., Stocchi, P., Tölle, M., Truhetz, H., Vautard, R., de Vries, H. and Warrach-Sagi,
785 K.: A first-of-its-kind multi-model convection permitting ensemble for investigating convective phenomena over
786 Europe and the Mediterranean, *Clim. Dynam.*, 1-32, <https://doi.org/10.1007/s00382-018-4521-8>, 2018.

787

788 Dahlgren, P., Landelius, T., Kållberg, P. and Gollvik, S., A high-resolution regional reanalysis for Europe. Part 1:
789 Three-dimensional reanalysis with the regional High-Resolution Limited-Area Model (HIRLAM), *Q.J.R. Meteorol.*
790 *Soc.*, 142, 2119-2131, doi:10.1002/qj.2807, 2016

791

792 Davini, P., Corti, S., D'Andrea, F., Rivière, G., and von Hardenberg, J.: Improved Winter European Atmospheric
793 Blocking Frequencies in High-Resolution Global Climate Simulations. *J. Adv. Model. Earth Syst.*, 9, 2615–2634,
794 <https://doi.org/10.1002/2017MS001082>, 2017a.

795

796 Davini, P., von Hardenberg, J., Corti, S., Christensen, H. M., Juricke, S., Subramanian, A., Watson, P. A. G.,
797 Weisheimer, A., and Palmer, T. N.: Climate SPHINX: evaluating the impact of resolution and stochastic physics
798 parameterisations in the EC-Earth global climate model, *Geosci. Model Dev.*, 10, 1383-1402,
799 <https://doi.org/10.5194/gmd-10-1383-2017>, 2017b.

800

801 Davini, P., and D'Andrea, F.: From CMIP-3 to CMIP-6: Northern Hemisphere atmospheric blocking simulation in
802 present and future climate. *J. Climate*, doi: <https://doi.org/10.1175/JCLI-D-19-0862.1>, 2020

803

804 Dawson, A. and Palmer, T. N.: Simulating weather regimes: impact of model resolution and stochastic
805 parameterization. *Clim Dynam*, 44, 2177-2193, <https://doi.org/10.1007/s00382-014-2238-x>, 2015.

806

807 Dawson, A., Palmer, T. N., and Corti, S.: Simulating regime structures in weather and climate prediction models,
808 *Geophys. Res. Lett.*, 39, L21805, <https://doi.org/10.1029/2012GL053284>, 2012.

809

810 Dee, D. P., Uppala, S. M., Simmons, A. J., Berrisford, P., Poli, P., Kobayashi, S., Andrae, U., Balmaseda, M. A.,
811 Balsamo, G., Bauer, P., Bechtold, P., Beljaars, A. C., van de Berg, L., Bidlot, J., Bormann, N., Delsol, C., Dragani, R.,
812 Fuentes, M., Geer, A. J., Haimberger, L., Healy, S. B., Hersbach, H., Hólm, E. V., Isaksen, L., Kållberg, P., Köhler,
813 M., Matricardi, M., McNally, A. P., Monge-Sanz, B. M., Morcrette, J., Park, B., Peubey, C., de Rosnay, P., Tavolato,
814 C., Thépaut, J. and Vitart, F.: The ERA-Interim reanalysis: Configuration and performance of the data assimilation
815 system, *Q. J. R. Meteorol. Soc.*, 137, 553–597, <https://doi.org/10.1002/qj.828>, 2011.

816

817 Demory, M. E., Vidale, P. L., Roberts, M. J., Berrisford, P., Strachan, J., Schiemann, R., and Mizielinski, M. S.: The
818 role of horizontal resolution in simulating drivers of the global hydrological cycle, *Clim. Dynam.*, 42, 2201–2225,
819 <https://doi.org/10.1007/s00382-013-1924-4>, 2014.

820
821 Demory, M.-E., Berthou, S., Sørland, S. L., Roberts, M. J., Beyerle, U., Seddon, J., Haarsma, R., Schär, C.,
822 Christensen, O. B., Fealy, R., Fernandez, J., Nikulin, G., Peano, D., Putrasahan, D., Roberts, C. D., Steger, C.,
823 Teichmann, C., and Vautard, R.: Can high-resolution GCMs reach the level of information provided by 12–50 km
824 CORDEX RCMs in terms of daily precipitation distribution?, *Geosci. Model Dev. Discuss.*,
825 <https://doi.org/10.5194/gmd-2019-370>, in review, 2020.
826
827 Donat M. G., Leckebusch G. C., Wild S., Ulbrich U.: Benefits and limitations of regional multi-model ensembles for
828 storm loss estimations, *Clim. Res.*, 44, 211-225. <https://doi.org/10.3354/cr00891>, 2010.
829
830 Donlon, C. J., Martin, M., Stark, J., Roberts-Jones, J., Fiedler, E., and Wimmer, W.: The Operational Sea Surface
831 Temperature and Sea Ice Analysis (OSTIA) system, *Remote Sens. Environ.*, 116, 140–158,
832 [doi:10.1016/j.rse.2010.10.017](https://doi.org/10.1016/j.rse.2010.10.017), 2012.
833
834 Eyring, V., Bony, S., Meehl, G. A., Senior, C. A., Stevens, B., Stouffer, R. J., and Taylor, K. E.: Overview of the
835 Coupled Model Intercomparison Project Phase 6 (CMIP6) experimental design and organization, *Geosci. Model Dev.*,
836 9, 1937–1958, <https://doi.org/10.5194/gmd-9-1937-2016>, 2016.
837
838 Fabiano, F., Christensen, H.M., Strommen, K., Athanasiadis, P., Baker, A., Schiemann, R. and Corti, S: Euro-Atlantic
839 weather Regimes in the PRIMAVERA coupled climate simulations: impact of resolution and mean state biases on
840 model performance. *Clim Dyn* 54, 5031–5048. <https://doi.org/10.1007/s00382-020-05271-w>, 2020
841
842 Fantini, A., Raffaele, F., Torma, C., Bacer, S., Coppola, E., Giorgi, F., Ahrens, B., Dubois, C., Sanchez, E. and
843 Verdecchia, M.: Assessment of multiple daily precipitation statistics in ERA-Interim driven Med-CORDEX and
844 EURO-CORDEX experiments against high resolution observations. *Clim Dyn* **51**, 877–900.
845 <https://doi.org/10.1007/s00382-016-3453-4>, 2018
846
847 Førland, E. and Institut, N. M.: Manual for Operational Correction of Nordic Precipitation Data. Norwegian
848 Meteorological Institute., 1996.
849
850 Gao, J., G., Shoshiro, M., Roberts, M. J., Haarsma, R., Putrasahan, D., Roberts, C. D., Scoccimarro, E., Terray, L.,
851 Vannièrè, B. and Vidale, P. L.: Influence of model resolution on bomb cyclones revealed by HighResMIP-
852 PRIMAVERA simulations, *Environ. Res. Lett.* 15, 084001, <https://doi.org/10.1088/1748-9326/ab88fa>, 2020
853
854 Giorgi F., Jones C., Asrar G. R.: Addressing climate information needs at the regional level: the CORDEX framework,
855 *WMO Bull.*, 58:175–183, 2009.
856

857 Goodison, B. E., Louie, P. Y. and Yang, D.: The WMO solid precipitation measurement intercomparison. World
858 Meteorological Organization-Publications-WMO TD, Report No. 67, 65–70, 1997.

859

860 Gutjahr, O., Schefczyk, L., Reiter, P. and Heinemann, G.: Impact of the horizontal resolution on the simulation of
861 extremes in COSMO-CLM, *Meteorol. Z.*, 25, 543 – 562, doi: 10.1127/metz/2016/0638, 2016.

862

863 Haarsma, R. J., Roberts, M. J., Vidale, P. L., Senior, C. A., Bellucci, A., Bao, Q., Chang, P., Corti, S., Fuckar, N. S.,
864 Guemas, V., von Hardenberg, J., Hazeleger, W., Kodama, C., Koenigk, T., Leung, L. R., Lu, J., Luo, J.-J., Mao, J.,
865 Mizielinski, M. S., Mizuta, R., Nobre, P., Satoh, M., Scoccimarro, E., Semmler, T., Small, J., and von Storch, J.-S.:
866 High Resolution Model Intercomparison Project (HighResMIP v1.0) for CMIP6, *Geosci. Model Dev.*, 9, 4185-4208,
867 <https://doi.org/10.5194/gmd-9-4185-2016>, 2016.

868

869 Hart, N. C. G., Washington, R., and Stratton, R. A.: Stronger local overturning in convective-permitting regional
870 climate model improves simulation of the subtropical annual cycle. *Geophys. Res. Lett.*, 45, 11334–11342,
871 <https://doi.org/10.1029/2018GL079563>, 2018.

872

873 Haylock, M. R., Hofstra, N., Klein Tank, A. M. G., Klok, E. J., Jones, P. D., New, M.: A European daily high-resolution
874 gridded data set of surface temperature and precipitation for 1950-2006. *J. Geophys. Res. Atmos.*, 113, D20119.
875 doi:10.1029/2008JD010201, 2008.

876

877 Herrera, S., Cardoso, R. M., Soares, P. M., Espírito-Santo, F., Viterbo, P., and Gutiérrez, J. M.: Iberia01: a new gridded
878 dataset of daily precipitation and temperatures over Iberia, *Earth Syst. Sci. Data*, 11, 1947–1956,
879 <https://doi.org/10.5194/essd-11-1947-2019>, 2019.

880

881 Herrmann, M., Somot, S., Calmanti, S., Dubois, C., and Sevault, F.: Representation of spatial and temporal variability
882 of daily wind speed and of intense wind events over the Mediterranean Sea using dynamical downscaling: impact of
883 the regional climate model configuration, *Nat. Hazards Earth Syst. Sci.*, 11, 1983-2001, [https://doi.org/10.5194/nhess-](https://doi.org/10.5194/nhess-11-1983-2011)
884 [11-1983-2011](https://doi.org/10.5194/nhess-11-1983-2011), 2011.

885

886 Hersbach, H., Bell, B., Berrisford, P., Horányi, A., Muñoz-Sabater, J., Nicolas, J., Radu, R., Schepers, D., Simmons,
887 A., Soci, C., Dee, D.: Global reanalysis: goodbye ERA-Interim, hello ERA5. ECMWF, doi:10.21957/vf291hehd7.
888 <https://www.ecmwf.int/node/19027>, 2019

889

890 Jacob, D., Petersen, J., Eggert, B., Alias, A., Christensen, O. B., Bouwer, L. M., Braun, A., Colette, A., Déqué, M.,
891 Georgievski, G., Georgopoulou, E., Gobiet, A., Menut, L., Nikulin, G., Haensler, A., Hempelmann, N., Jones, C.,
892 Keuler, K., Ko-vats, S., Kröner, N., Kotlarski, S., Kriegsmann, A., Martin, E., Meijgaard, E. van, Moseley, C., Pfeifer,
893 S., Preuschmann, S., Radermacher, C., Radtke, K., Rechid, D., Rounsevell, M., Samuelsson, P., Somot, S., Soussana,
894 J.-F., Teichmann, C., Valentini, R., Vautard, R., Weber, B., and Yiou, P.: EURO-CORDEX: new high-resolution

895 climate change projections for European impact research, *Reg. Environ. Change*, 14, 563–578, doi:10.1007/s10113-
896 013-0499-2, 2014.

897

898 Jacob, D., Teichmann, C., Sobolowski, S. *et al.* Regional climate downscaling over Europe: perspectives from the
899 EURO-CORDEX community. *Reg Environ Change*, **20**, 51, <https://doi.org/10.1007/s10113-020-01606-9>, 2020

900

901 Jézéquel, A., Yiou, P. and Radanovics, S.: Role of circulation in European heatwaves using flow analogues. *Clim.*
902 *Dynam.* 50, 1145-1159, <https://doi.org/10.1007/s00382-017-3667-0>, 2018.

903

904 Jourdiar, B.: Evaluation of ERA5, MERRA-2, COSMO-REA6, NEWA and AROME to simulate wind power
905 production over France, *Adv. Sci. Res.*, 17, 63–77, <https://doi.org/10.5194/asr-17-63-2020>, 2020.

906

907 Jung, T., Gulev, S. K., Rudeva, I. and Soloviov, V.: Sensitivity of extratropical cyclone characteristics to horizontal
908 resolution in the ECMWF model. *Q.J.R. Meteorol. Soc.*, 132, 1839-1857, doi:10.1256/qj.05.212, 2006.

909

910 Jung, T., Miller, M. J., Palmer, T. N., Towers, P., Wedi, N., Achuthavarier, D., Adams, J. M., Altshuler, E. L., Cash,
911 B. A., Kinter, J. L., Marx, L., Stan, C., and Hodges, K. I.: High-Resolution Global Climate Simulations with the
912 ECMWF Model in Project Athena: Experimental Design, Model Climate, and Seasonal Forecast Skill, *J. Climate.*, 25,
913 3155–3172, doi:10.1175/JCLI-D-11-00265.1, 2012.

914

915 Kendon, E. J., Roberts, N. M., Senior, C. A., and Roberts, M. J.: Realism of rainfall in a very high-resolution regional
916 climate model, *J. Climate.*, 25, 5791–5806. doi: 10.1175/JCLI-D-11-00562.1, 2012.

917

918 Kendon, E. J., Roberts, N. M., Fowler, H. J., Roberts, M. J., Chan, S. C., and Senior, C. A.: Heavier summer downpours
919 with climate change revealed by weather forecast resolution model, *Nat. Clim. Change*, 4, 570–576, doi:
920 10.1038/nclimate2258, 2014.

921

922 Kendon, E. J., Ban, N., Roberts, N. M., Fowler, H. J., Roberts, M. J., Chan, S. C., Evans, J. P., Fosser, G. and
923 Wilkinson, J.M.: Do Convection-Permitting Regional Climate Models Improve Projections of Future Precipitation
924 Change?. *B. Am. Meteorol. Soc.*, 98, 79–93, <https://doi.org/10.1175/BAMS-D-15-0004.1>, 2017.

925

926 Klaver, R., Haarsma, R., Vidale, P. L., Hazeleger, W.: Effective resolution in high resolution global atmospheric
927 models for climate studies. *Atmos Sci Lett.*, 1– 8. <https://doi.org/10.1002/asl.952>, 2020

928

929 Kopparla, P., Fischer, E. M., Hannay, C., and Knutti, R.: Improved simulation of extreme precipitation in a high-
930 resolution atmosphere model, *Geophys. Res. Lett.*, 40, 5803-5808, doi: 10.1002/2013GL057866, 2013.

931

932 Kotlarski, S., Keuler, K., Christensen, O. B., Colette, A., Déqué, M., Gobiet, A., Goergen, K., Jacob, D., Lüthi, D.,
933 van Meijgaard, E., Nikulin, G., Schär, C., Teichmann, C., Vautard, R., Warrach-Sagi, K., and Wulfmeyer, V.: Regional
934 climate modeling on European scales: a joint standard evaluation of the EURO-CORDEX RCM ensemble, *Geosci.*
935 *Model Dev.*, 7, 1297–1333, <https://doi.org/10.5194/gmd-7-1297-2014>, 2014.

936

937 Kunz, M., Mohr, S., Rauthe, M., Lux, R., and Kottmeier, C.: Assessment of extreme wind speeds from Regional
938 Climate Models – Part 1: Estimation of return values and their evaluation, *Nat. Hazards Earth Syst. Sci.*, 10, 907-922,
939 <https://doi.org/10.5194/nhess-10-907-2010>, 2010.

940

941 Landelius, T., Dahlgren, P., Gollvik, S., Jansson, A. and Olsson, E.: A high-resolution regional reanalysis for Europe.
942 Part 2: 2D analysis of surface temperature, precipitation and wind, *Q. J. R. Meteorol. Soc.*, 142, 2132–2142,
943 doi:10.1002/qj.2813, 2016.

944

945 Lhotka, O., Kyselý, J. and Farda, A.: Climate change scenarios of heat waves in Central Europe and their uncertainties.
946 *Theor Appl Climatol.*, 131, 1043-1054, <https://doi.org/10.1007/s00704-016-2031-3>, 2018.

947

948 Matsueda, M., Mizuta, R. and Kusunoki, S.: Future change in wintertime atmospheric blocking simulated using a 20-
949 km-mesh atmospheric global circulation model, *J. Geophys. Res.*, 114, D12114, doi: 10.1029/2009JD011919, 2009.

950

951 Mizielinski, M. S., Roberts, M. J., Vidale, P. L., Schiemann, R., Demory, M.-E., Strachan, J., Edwards, T., Stephens,
952 A., Lawrence, B. N., Pritchard, M., Chiu, P., Iwi, A., Churchill, J., del Cano Novales, C., Kettleborough, J., Roseblade,
953 W., Selwood, P., Foster, M., Glover, M., and Malcolm, A.: High-resolution global climate modelling: the UPSCALE
954 project, a large-simulation campaign, *Geosci. Model Dev.*, 7, 1629–1640, doi:10.5194/gmd-7-1629-2014, 2014.

955

956 Niermann, D., Kaiser-Weiss, A., Borsche, M., van den Besselaar, E., Lussana, C., Isotta, F., Frei, C, Cantarello, L.,
957 Tveito, O. E., van der Schrier, G., Cornes, R, Vreede, E., Bojariu, R, and Davie, J.: Report for Deliverable 3.6 of the
958 UERRA project: Scientific report on assessment of regional analysis against independent data sets, pp. 138 , available
959 from: <http://www.uerra.eu/publications/deliverable-reports.html>

960

961 O'Brien, T. A., Collins, W. D., Kashinath, K., Rübel, O., Byna, S., Gu, J., Krishnan, H. and Ullrich, P. A.: Resolution
962 dependence of precipitation statistical fidelity in hindcast simulations, *J. Adv. Model. Earth Syst.*, 8, 976–990, doi:
963 10.1002/2016MS000671, 2016.

964

965 O'Reilly, C. H., Minobe, S. and Kuwano-Yoshida, A.: The influence of the Gulf Stream on wintertime European
966 blocking, *Clim. Dynam.*, 47, 1545- 1567, <https://doi.org/10.1007/s00382-015-2919-0>, 2016.

967

968 Prein, A. F. and Gobiet, A.: Impacts of uncertainties in European gridded precipitation observations on regional climate
969 analysis, *Int. J. Climatol.*, 37, 305-327, doi:10.1002/joc.4706, 2017.

970
971 Prein, A. F., Langhans, W., Fossier, G., Ferrone, A., Ban, N., Goergen, K., Keller, M., Tölle, M., Gutjahr, O., Feser,
972 F., Brisson, E., Kollet, S., Schmidli, J., Van Lipzig, N. P. M., and Leung, R.: A review on regional convection-
973 permitting climate modeling: Demonstrations, prospects, and challenges, *Rev. Geophys.*, 53, 323–361. doi:
974 10.1002/2014RG000475, 2015.
975
976 Prein, A.F., Gobiet, A., Truhetz, H., Keuler, K., Goergen, K., Teichmann, C., Fox Maule, C., van Meijgaard, E., Déqué,
977 M., Nikulin, G., Vautard, R., Colette, A., Kjellström, E., and Jacob, D.: Precipitation in the EURO-CORDEX 0.11°
978 and 0.44° simulations: high resolution, high benefits?, *Clim. Dynam.* 46, 383-412, doi: 10.1007/s00382-015-2589-y,
979 2016.
980
981 Pryor, S. C., Nikulin, G., and Jones, C.: Influence of spatial resolution on regional climate model derived wind climates,
982 *J. Geophys. Res.*, 117, D03117, doi:10.1029/2011JD016822, 2012
983
984 Risanto, C.B., Castro, C.L., Moker, J.M., Jr., Arellano, A.F., Jr., Adams, D.K., Fierro, L.M., Minjarez Sosa, C.M.:
985 Evaluating Forecast Skills of Moisture from Convective-Permitting WRF-ARW Model during 2017 North
986 American Monsoon Season. *Atmosphere*, 10, 694, doi:[10.3390/atmos10110694](https://doi.org/10.3390/atmos10110694), 2019
987
988 Roberts, M. J., Vidale, P. L., Senior, C., Hewitt, H. T., Bates, C., Berthou, S., Chang, P., Christensen, H. M., Danilov,
989 S., Demory, M. E., Griffies, S. M., Haarsma, R., Jung, T., Martin, G., Minobe, S., Ringler, T., Satoh, M., Schiemann,
990 R., Scoccimarro, E., Stephens, G. and Wehner, M.F.: The benefits of global high-resolution for climate simulation:
991 process-understanding and the enabling of stakeholder decisions at the regional scale.. *B. Am. Meteorol. Soc.*, 99,
992 2341–2359 <https://doi.org/10.1175/BAMS-D-15-00320.1>, 2018.
993
994 Ruti, P. M., Somot, S., Giorgi, F., Dubois, C., Flaounas, E., Obermann, A., Dell’Aquila, A., Pisacane, G., Harzallah,
995 A., Lombardi, E., Ahrens, B., Akhtar, N., Alias, A., Arsouze, T., Aznar, R., Bastin, S., Bartholy, J., Béranger, K.,
996 Beuvier, J., Bouffies-Cloch e, S., Brauch, J., Cabos, W., Calmanti, S., Calvet, J., Carillo, A., Conte, D., Coppola, E.,
997 Djurdjevic, V., Drobinski, P., Elizalde-Arellano, A., Gaertner, M., Gal n, P., Gallardo, C., Gualdi, S., Goncalves, M.,
998 Jorba, O., Jord , G., L’Heveder, B., Lebeaupin-Brossier, C., Li, L., Liguori, G., Lionello, P., Maci s, D., Nabat, P.,
999  nol, B., Raikovic, B., Ramage, K., Sevault, F., Sannino, G., Struglia, M. V., Sanna, A., Torma, C., and Vervatis, V.:
1000 Med-CORDEX Initiative for Mediterranean Climate Studies. *B. Am. Meteorol. Soc.*, 97, 1187–1208,
1001 <https://doi.org/10.1175/BAMS-D-14-00176.1>, 2016
1002
1003 Schiemann, R., Demory, M. E., Shaffrey, L. C., Strachan, J., Vidale, P. L., Mizielinski, M. S., Roberts, M. J., Matsueda,
1004 M., Wehner, M. F. and Jung, T.: The resolution sensitivity of Northern Hemisphere blocking in four 25-km
1005 atmospheric global circulation models, *J. Climate.*, 30, 337–358, <https://doi.org/10.1175/JCLI-D-16-0100.1>, 2017.
1006

1007 Schiemann, R., Vidale, P. L., Shaffrey, L. C., Johnson, S. J., Roberts, M. J., Demory, M.-E., Mizielinski, M. S., and
1008 Strachan, J.: Mean and extreme precipitation over European river basins better simulated in a 25 km AGCM, *Hydrol.*
1009 *Earth Syst. Sci.*, 22, 3933-3950, <https://doi.org/10.5194/hess-22-3933-2018>, 2018.

1010

1011 Schiemann, R., Athanasiadis, P., Barriopedro, D., Doblas-Reyes, F., Lohmann, K., Roberts, M. J., Sein, D. V., Roberts,
1012 C. D., Terray, L., and Vidale, P. L.: Northern Hemisphere blocking simulation in current climate models: evaluating
1013 progress from the Climate Model Intercomparison Project Phase 5 to 6 and sensitivity to resolution, *Weather Clim.*
1014 *Dynam.*, 1, 277–292, <https://doi.org/10.5194/wcd-1-277-2020>, 2020.

1015

1016 Seneviratne, S. I., Nicholls, N., Easterling, D., Goodess, C. M., Kanae, S., Kossin, J., Luo, Y., Marengo, J., McInnes,
1017 K., Rahimi, M., Reichstein, M., Sorteberg, A., Vera, C. and Zhang, X.: Changes in climate extremes and their impacts
1018 on the natural physical environment. In: *Managing the Risks of Extreme Events and Disasters to Advance Climate*
1019 *Change Adaptation. A Special Report of Working Groups I and II of the Intergovernmental Panel on Climate Change*,
1020 edited by: Field, C. B., Barros, V., Stocker, T. F., Qin, D., Dokken, D. J., Ebi, K., L. Mastrandrea, M. D., Mach, K.
1021 J., Plattner, G.-K., Allen, S. K., Tignor, M. and Midgley, P. M., Cambridge University Press, Cambridge, UK, and
1022 New York, NY, USA, pp. 109-230, 2012

1023

1024 Shields, C. A., Kiehl, J. T., and Meehl, G. A.: Future changes in regional precipitation simulated by a half-degree
1025 coupled climate model: Sensitivity to horizontal resolution, *J. Adv. Model. Earth Syst.*, 8, 863–884, doi:
1026 10.1002/2015MS000584, 2016.

1027

1028 Skamarock, W.C.: Evaluating Mesoscale NWP Models Using Kinetic Energy Spectra. *Mon. Wea. Rev.*, 132, 3019–
1029 3032, <https://doi.org/10.1175/MWR2830.1>, 2004

1030

1031 Strandberg, G. and Lind, P.: The importance of model resolution on simulated precipitation in Europe – from global
1032 to regional model, *Weather Clim. Dynam. Discuss.*, <https://doi.org/10.5194/wcd-2020-31>, in review, 2020.

1033

1034 Stott, P. A., Christidis, N., Otto, F. E., Sun, Y., Vanderlinden, J., van Oldenborgh, G. J., Vautard, R., von Storch, H.,
1035 Walton, P., Yiou, P. and Zwiers, F. W.: Attribution of extreme weather and climate-related events. *WIREs Clim.*
1036 *Change*, 7, 23-41. doi:10.1002/wcc.380, 2016.

1037

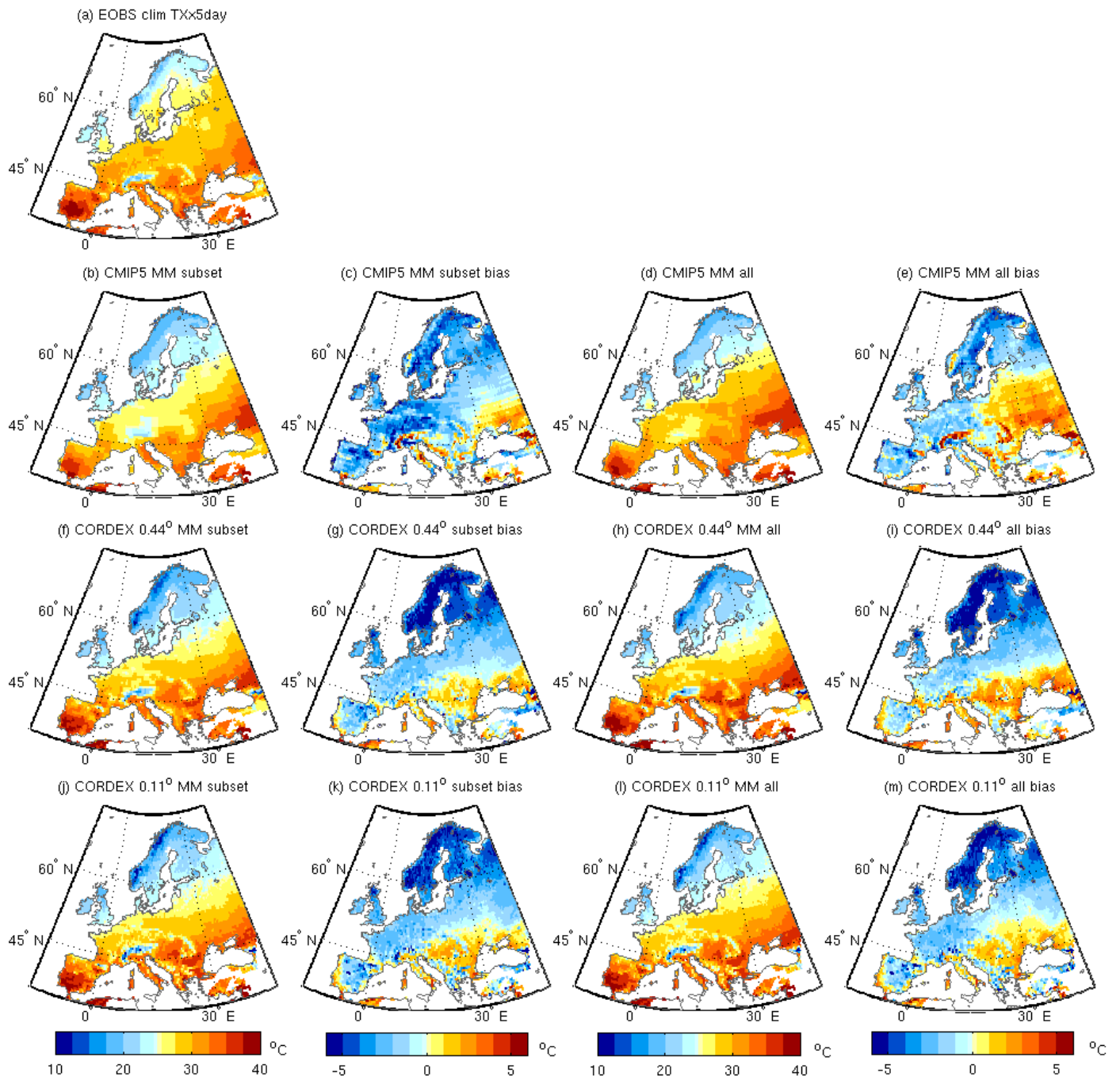
1038 Strommen, K., Mavilia, I., Corti, S., Matsueda, M., Davini, P., von Hardenberg, J., Vidale, P.-L. and Mizuta, R. : The
1039 sensitivity of Euro-Atlantic regimes to model horizontal resolution. *Geophysical Research*
1040 *Letters*, 46, 7810– 7818. <https://doi.org/10.1029/2019GL082843>, 2019

1041

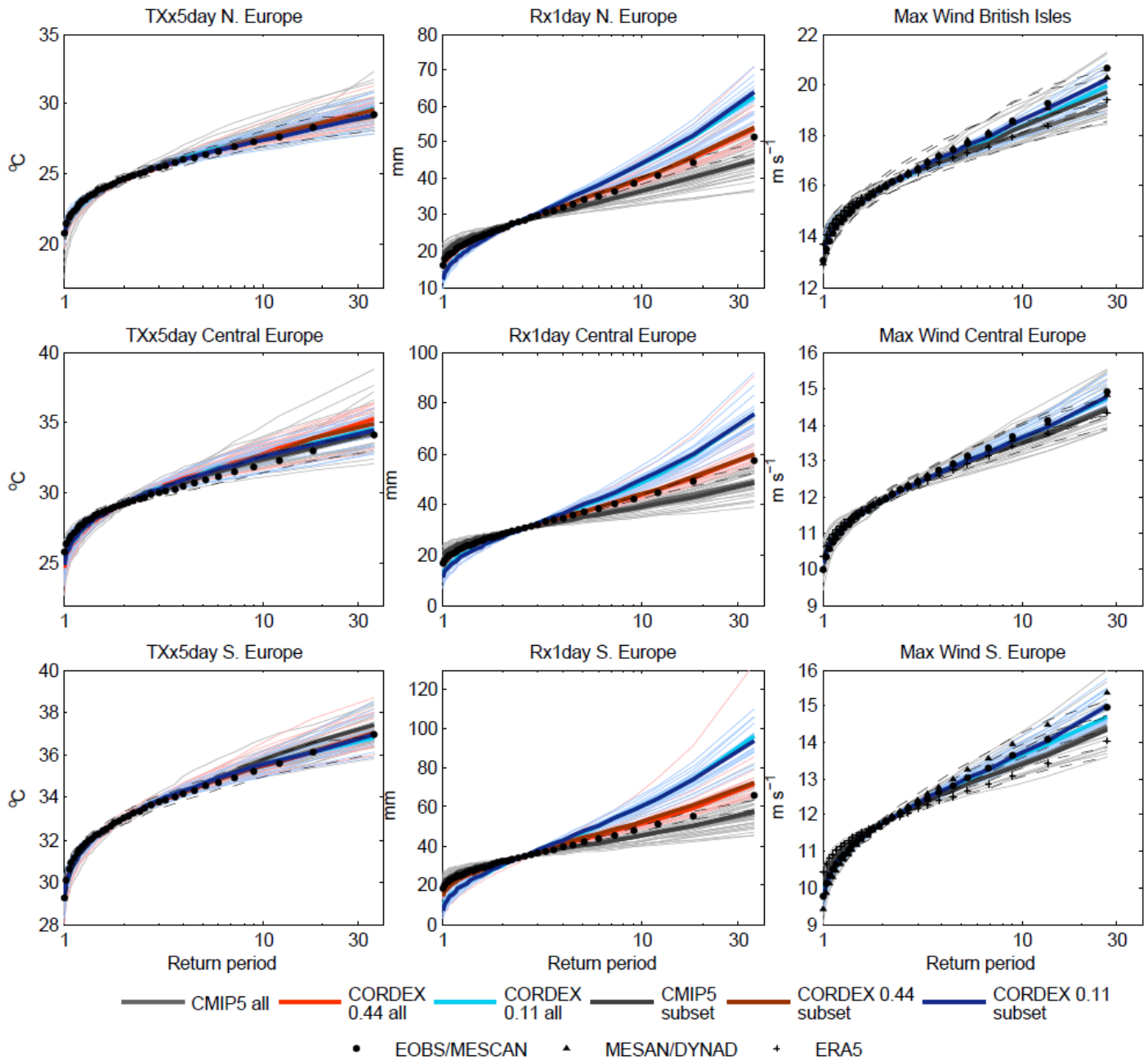
1042 Taylor, K., Williamson, D., and Zwiers, F.: The sea surface temperature and sea-ice concentration boundary conditions
1043 for AMIP II simulations, PCMDI Rep. 60, Tech. Rep. 60, PCMDI, 25 pp., available at: [http://www-](http://www-pcmdi.llnl.gov/publications/ab60.html)
1044 [pcmdi.llnl.gov/publications/ab60.html](http://www-pcmdi.llnl.gov/publications/ab60.html), 2000.

1045
1046 Taylor, K. E., Stouffer, R. J. and Meehl, G. A.: An overview of CMIP5 and the experiment design, *B. Am. Meteorol.*
1047 *Soc.*, 93, 485498, doi: 10.1175/BAMS-D-11-00094.1, 2012.
1048
1049 Terai, C. R., Caldwell, P. M., Klein, S. A. Tang, Q. and Branstetter, M. L.: The atmospheric hydrologic cycle in the
1050 ACME v0.3 model. *Clim. Dynam.*, 50, 3251- 3279. <https://doi.org/10.1007/s00382-017-3803-x>, 2018.
1051
1052 Torma, C., Giorgi, F. and Coppola, E.: Added value of regional climate modeling over areas characterized by complex
1053 terrain—Precipitation over the Alps, *J. Geophys. Res. Atmos.*, 120, 3957–3972, doi: 10.1002/2014JD022781, 2015.
1054
1055 van der Linden, E. C., Haarsma, R. J., and van der Schrier, G.: Impact of climate model resolution on soil moisture
1056 projections in central-western Europe, *Hydrol. Earth Syst. Sci.*, 23, 191–206, [https://doi.org/10.5194/hess-23-191-](https://doi.org/10.5194/hess-23-191-2019)
1057 2019, 2019.
1058
1059 Van Haren, R., Haarsma, R. J., Van Oldenborgh, G. J. and Hazeleger, W.: Resolution Dependence of European
1060 Precipitation in a State-of-the-Art Atmospheric General Circulation Model, *J. Climate.*, 28, 5134–5149, doi:
1061 10.1175/JCLI-D-14-00279.1, 2015a.
1062
1063 Van Haren, R., Haarsma, R. J., de Vries, H., van Oldenborgh, G. J., and Hazeleger, W.: Resolution dependence of
1064 circulation forced future central European summer drying, *Environ. Res. Lett.*, 10, 055002, doi:10.1088/1748-
1065 9326/10/5/055002, 2015b.
1066
1067 Vanniere, B., Vidale, P. L., Demory, M.-E., Schiemann, R., Roberts, M. J., Roberts, C. D., Matsueda, M., Terray, L.,
1068 Koenigk, T., Senan, R.: Multi-model evaluation of the sensitivity of the global energy budget and hydrological cycle
1069 to resolution, *Clim. Dynam.*, 52, 6817- 6846, <https://doi.org/10.1007/s00382-018-4547-y>, 2019
1070
1071 Vautard, R., Gobiet, A., Jacob, D., Belda, M., Colette, A., Déqué, M., Fernández, J., García-Díez, M., Goergen, K.,
1072 Güttler, I., Halenka, T., Karacostas, T., Katragkou, E., Keuler, K., Kotlarski, S., Mayer, S., van Meijgaard, E., Nikulin,
1073 G., Patarcic, M., Scinocca, J., Sobolowski, S., Suklitsch, M., Teichmann, C., Warrach-Sagi, K., Wulfmeyer, V., Yiou,
1074 P. : The simulation of European heat waves from an ensemble of regional climate models within the EURO-CORDEX
1075 project, *Clim. Dynam.*, 41, 2555-2575, doi: 10.1007/s00382-013-1714-z, 2013.
1076
1077 Vautard, R., Yiou, P., Otto, F., Stott, P., Christidis, N., van Oldenborgh, G. J. and Schaller, N.: Attribution of human-
1078 induced dynamical and thermodynamical contributions in extreme weather events, *Environ. Res. Lett.*, 11, 114009,
1079 <https://doi.org/10.1088/1748-9326/11/11/114009>, 2016.
1080

1081 Volosciuk, C., Maraun, D., Semenov, V.A. and Park, W.: Extreme Precipitation in an Atmosphere General Circulation
1082 Model: Impact of Horizontal and Vertical Model Resolutions, *J. Climate.*, 28, 1184–1205,
1083 <https://doi.org/10.1175/JCLI-D-14-00337.1>, 2015.
1084
1085 Vries, H. de, Scher, S., Haarsma, R., Drijfhout, S., and Delden, A. van.: How Gulf-Stream SST-fronts influence
1086 Atlantic winter storms, *Clim. Dynam.*, 52, 5899-5909. <https://doi.org/10.1007/s00382-018-4486-7>, 2019
1087
1088 Wehner, M. F., Smith, R. L., Bala, G. and Duffy, P.: The effect of horizontal resolution on simulation of very extreme
1089 US precipitation events in a global atmosphere model, *Clim. Dynam.*, 34, 241-247. [https://doi.org/10.1007/s00382-](https://doi.org/10.1007/s00382-009-0656-y)
1090 [009-0656-y](https://doi.org/10.1007/s00382-009-0656-y), 2010.
1091
1092 Wehner, M. F., Reed, K. A., Li, F., Prabhat, Bacmeister, J., Chen, C.-T., Paciorek, C., Gleckler, P. J., Sperber, K. R.,
1093 Collins, W. D., Gettelman, A., and Jablonowski, C.: The effect of horizontal resolution on simulation quality in the
1094 Community Atmospheric Model, CAM5.1, *J. Adv. Model. Earth Syst.*, 6, 980–997, doi:10.1002/2013MS000276,
1095 2014.
1096
1097 Willison, J., Robinson, W.A. and Lackmann, G.M.: North Atlantic Storm-Track Sensitivity to Warming Increases with
1098 Model Resolution., *J. Climate.*, 28, 4513–4524, <https://doi.org/10.1175/JCLI-D-14-00715.1>, 2015.
1099
1100 Zappa, G., Shaffrey, L. C. and Hodges, K. I., The Ability of CMIP5 Models to Simulate North Atlantic Extratropical
1101 Cyclones, *J. Climate.*, 26, 5379-5396, doi: 10.1175/JCLI-D-12-00501.1, 2013.
1102
1103 Zhang, X., Alexander, L., Hegerl, G. C., Jones, P., Tank, A. K., Peterson, T. C. Trewin, B. and Zwiers, F. W.: Indices
1104 for monitoring changes in extremes based on daily temperature and precipitation data, *Wiley Interdiscip. Rev., Clim.*
1105 *Chang.*, 2, 851–870, doi:10.1002/wcc.147, 2011.
1106



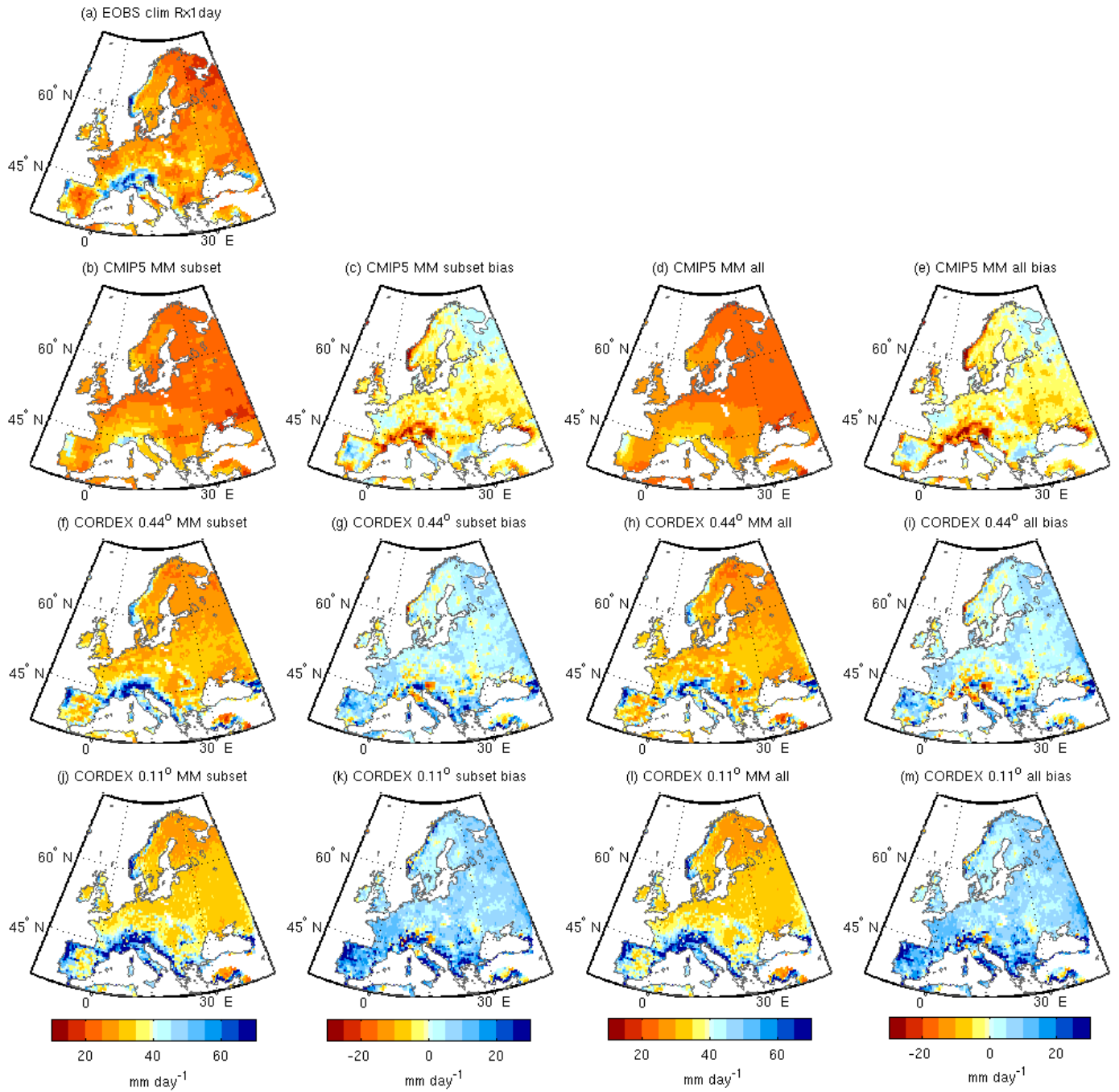
1108
 1109 **Figure 1: Climatological mean of TXx5day for the period 1970-2005 for (a) E-OBS; the multi model median of the common**
 1110 **subset of models (see Methods) for (b) CMIP5, (f) CORDEX 0.44° and (j) CORDEX 0.11°, (c, g, k) their biases with respect**
 1111 **to E-OBS, and (d,e,h,i,j,k) the same for the full ensembles of CMIP5 and CORDEX. Units °C.**



1113

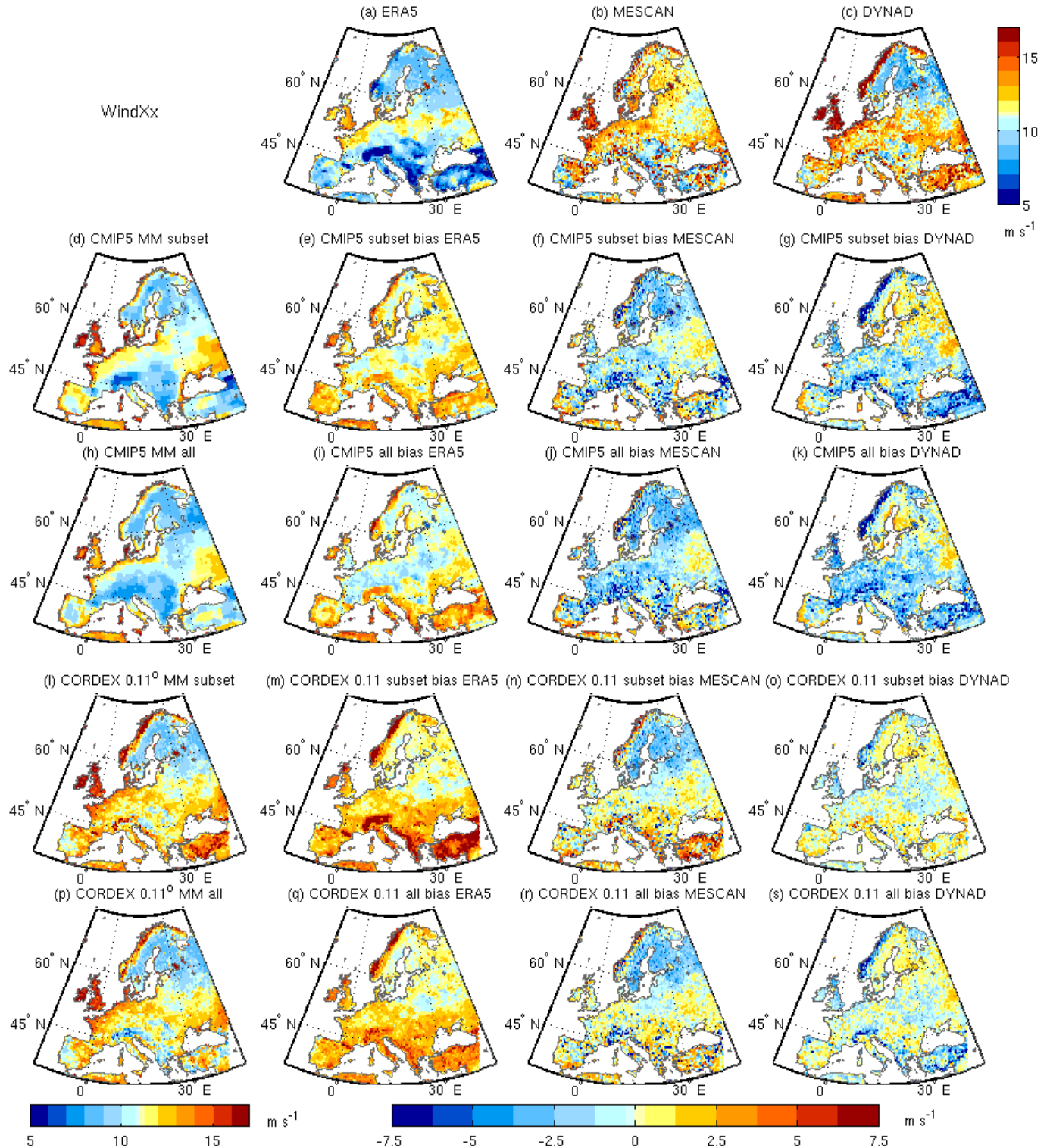
1114 **Figure 2: Return period plots for (left) TXx5day, (middle column) Rx1day and (right) annual maximum wind, for CMIP5**
 1115 **and CORDEX for Northern Europe (top row (except top right = British Isles)), Central Europe (middle row) and Southern**
 1116 **Europe (bottom row). CMIP5 is shown in grey, CORDEX 0.44° in red and CORDEX 0.11° in blue. Thin lines are individual**
 1117 **ensemble members, thick lines are multi model medians: lighter colours for the full ensembles, and darker colours for the**
 1118 **subset of models common to CMIP5 and both CORDEX resolutions. Observational datasets are shown in black, circles for**
 1119 **E-OBS temperature and precipitation and MESCAN wind, triangles for MESAN precipitation and DYNAD wind and**
 1120 **crosses for ERA5 wind. Confidence intervals based on bootstrapping are shown with dashed lines for the observational**
 1121 **datasets. The time periods considered are 1970-2005 for TXx5day and Rx1day, and 1979-2005 for wind.**

1122

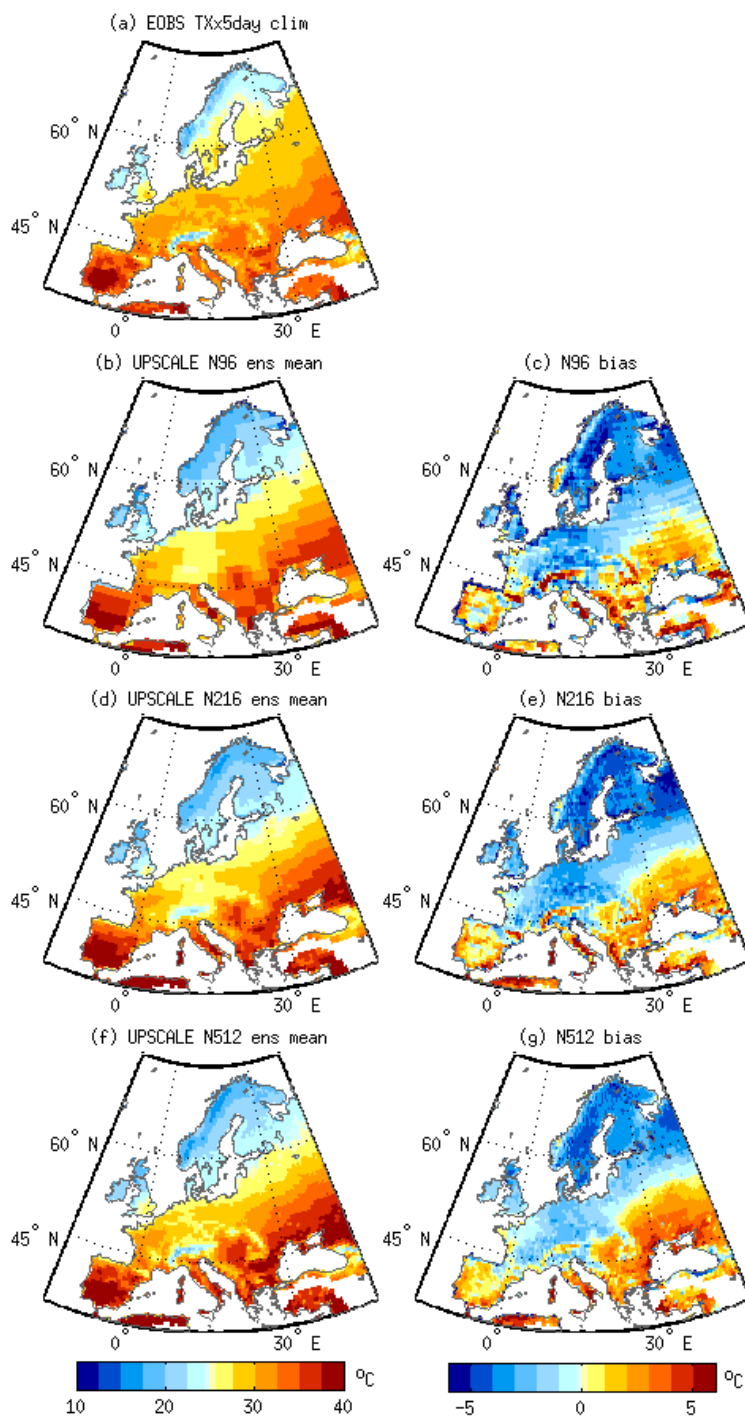


1123

1124 **Figure 3: As for Figure 1 but for the climatological mean of Rx1day. Units mm.**

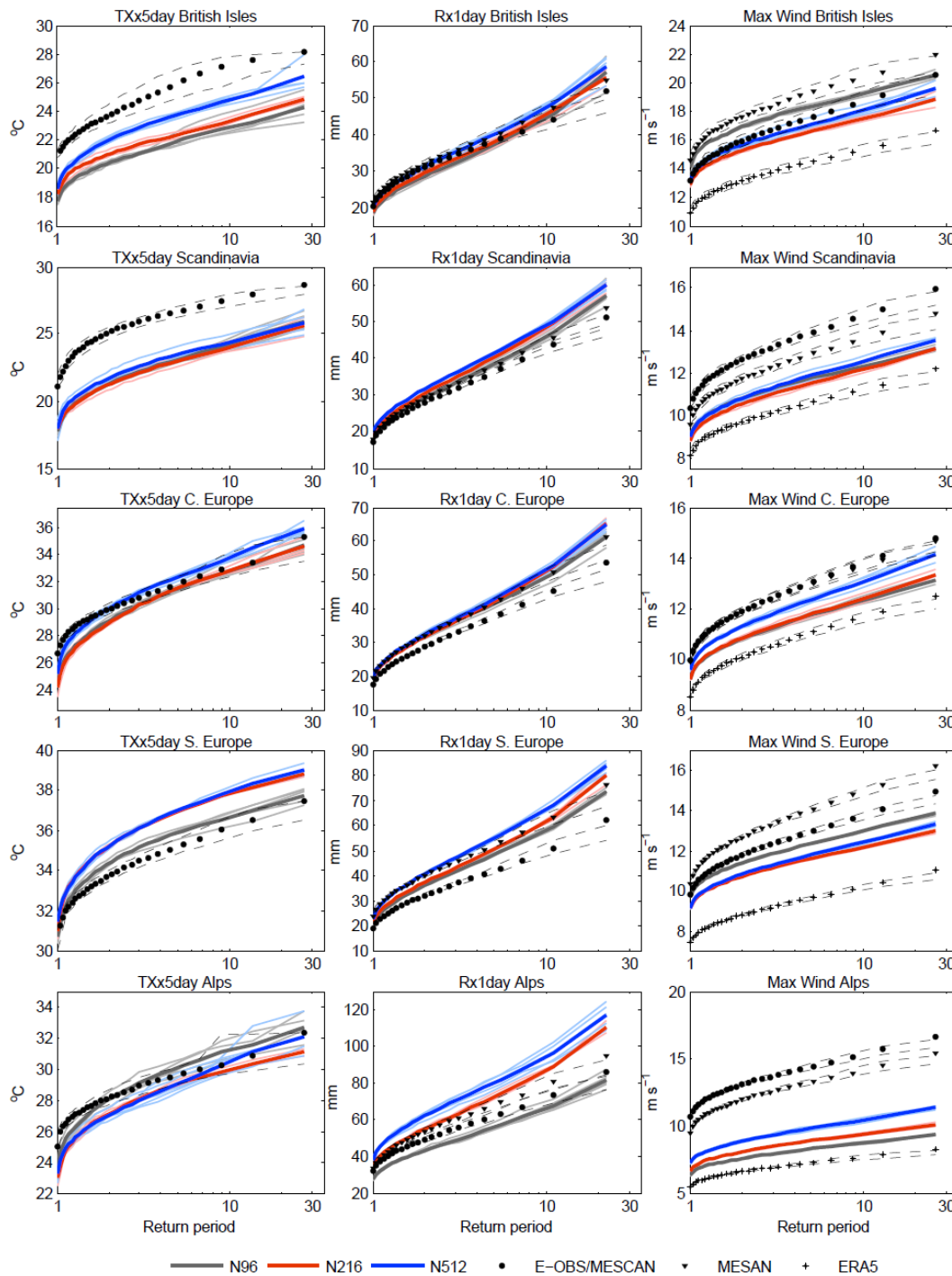


1125
 1126 **Figure 4: Climatological mean of annual maximum wind for the period 1979-2005 for (a) ERA5, (b) MESCAN (c)**
 1127 **DYNAD, and for the multi model median of the common subset of models for (d) CMIP5 and (l) CORDEX 0.11° and their**
 1128 **biases with respect to the reanalyses datasets (e-g and m-o). (h-k and p-s) are the same but for the full ensembles of**
 1129 **CMIP5 and CORDEX. Units meters per second.**



1130

Figure 5: Climatological mean of Txx5day for the ensemble means of three resolutions of HadGEM3-A (UPSCALE) GCM simulations (left) for the period 1985-2011 and their biases with respect to E-OBS (right). (a) E-OBS, (b, c) N96 (130 km), (d, e) N216 (60 km), (f, g) N512 (25 km). Units °C.



1135 **Figure 6:** Return period plots for (left) TXx5day, middle column Rx1day and (right) annual maximum wind, for the UPSCALE simulations for (top row) the British Isles, (2nd row) Scandinavia, (3rd row) Central Europe, (4th row) Southern Europe, and (last row) the Alps. N96 is shown in grey, N216 in red and N512 in blue. Thin lines are individual ensemble members, thick lines represent

ensemble means. Observational datasets are shown in black, circles for E-OBS and MESCAN, triangles for MESAN and DYNAD, and asterisks for ERA5. Confidence intervals based on bootstrapping are shown with dashed lines for the observational datasets. The time periods considered are 1985-2011 for TXx5day, 1989-2010 for Rx1day, and 1986-2011 for wind. NB: in contrast to Figure 2 the curves have not been shifted to have the same mean value (see methods), see Figure S10 for the shifted version.

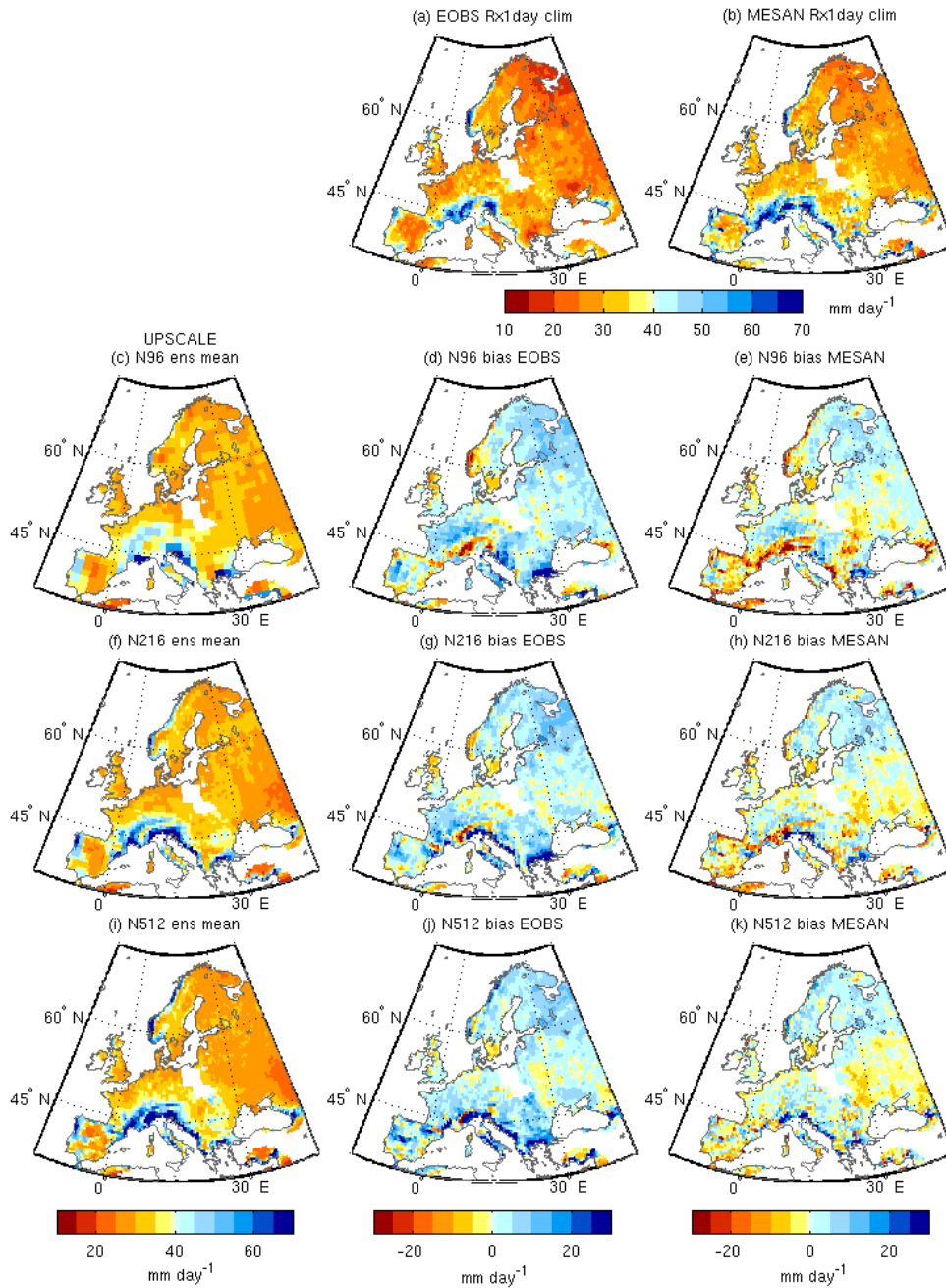


Figure 7: Climatological mean of Rx1day for the ensemble means of three resolutions of UPSCALE (left) simulations for the period 1989-2010 and their biases with respect to E-OBS (middle) and the MESAN reanalysis (right). (a) E-OBS, (b) MESAN (c-e) N96, (f-h) N216, (i-k) N512. Units mm.

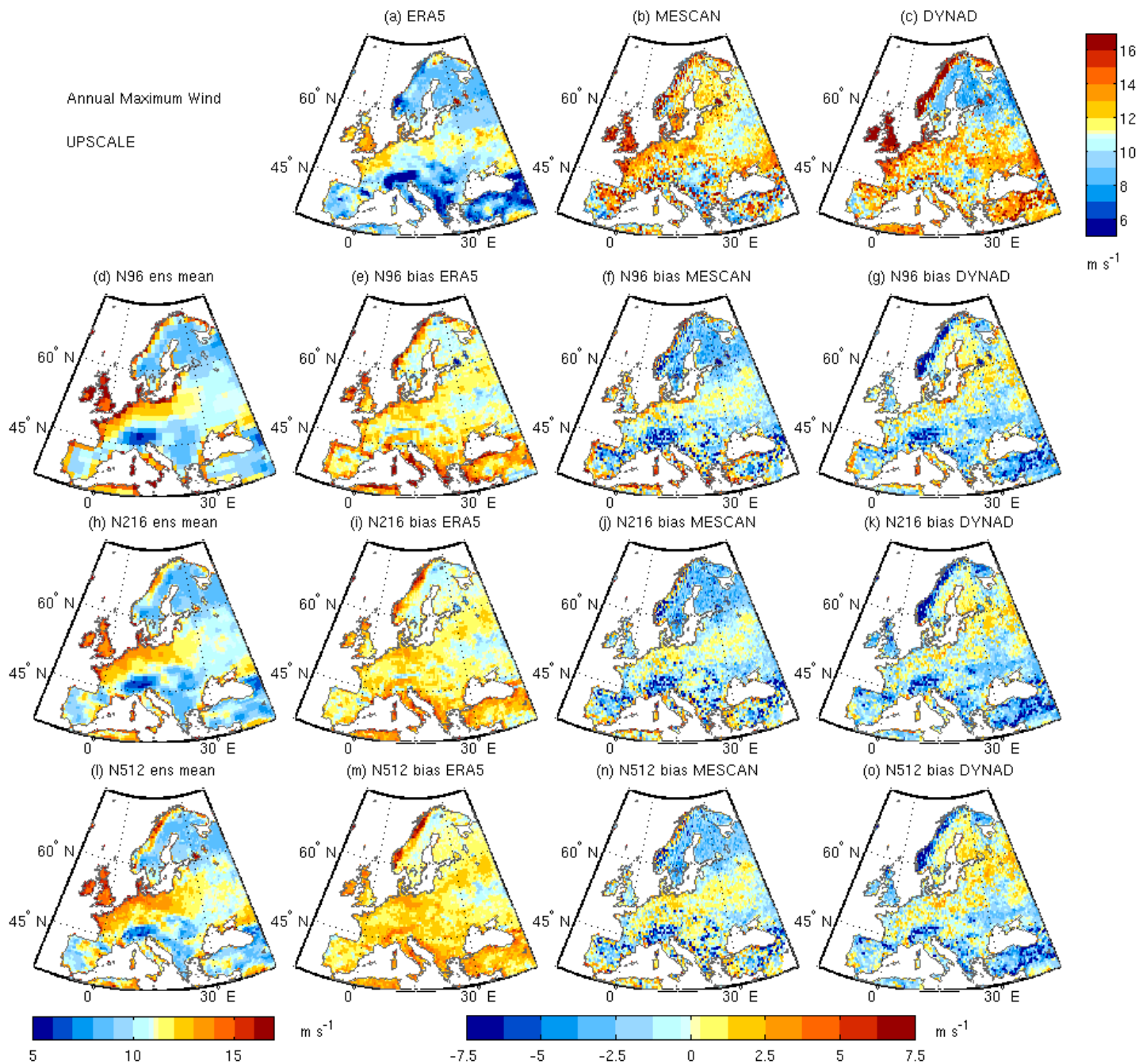
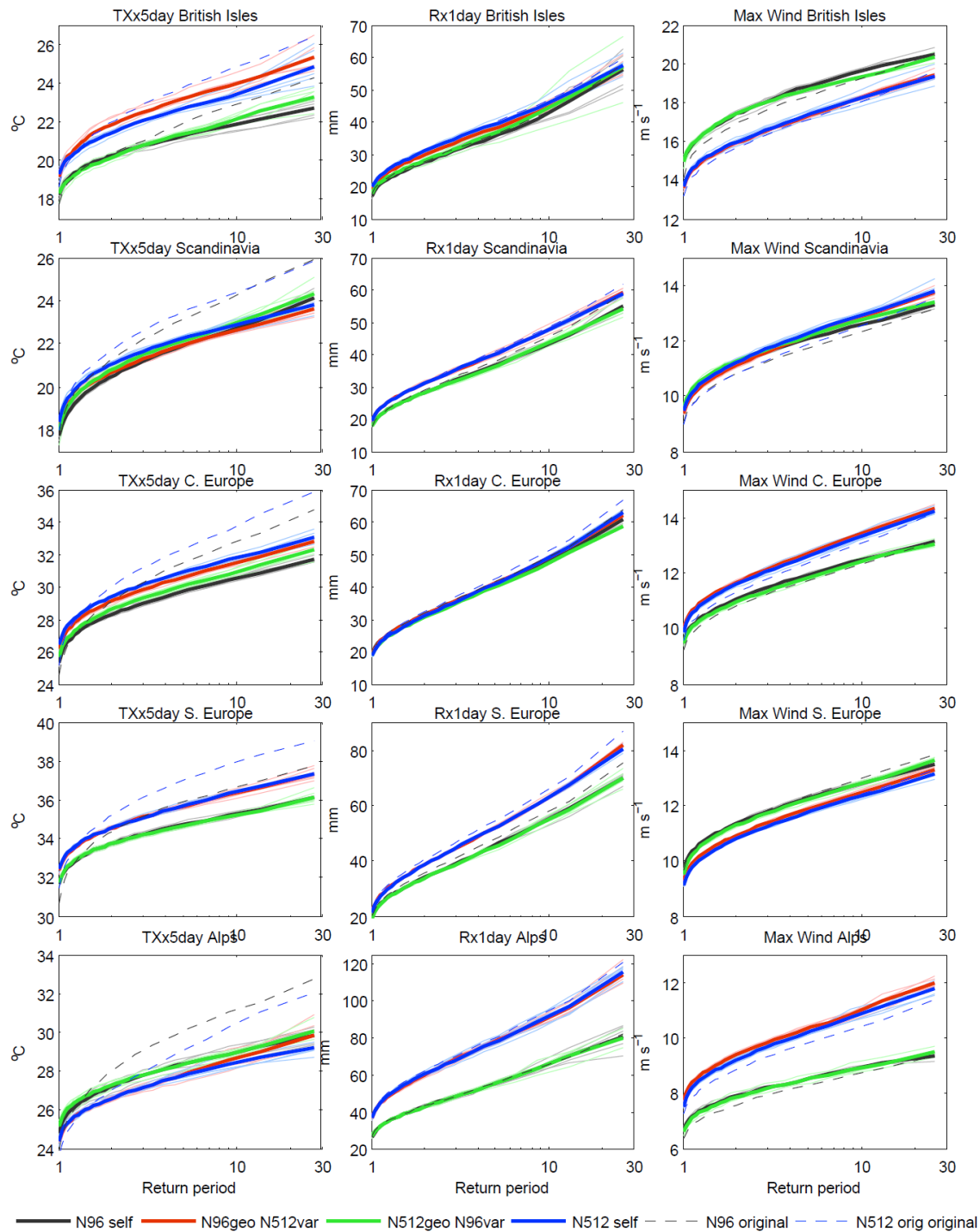


Figure 8: Climatological mean of annual maximum wind for the ensemble means of three resolutions of UPSCALE (left) simulations for the period 1986-2011 and their biases with respect to the observational datasets ERA5 (left column), MESCAN (middle) and MESAN (right). (a) ERA5, (b) MESCAN (c) DYNAD, (d-g) N96, (h-k) N216, (l-o) N512. Units meters per second.



1150 **Figure 9: Circulation analogue results. Return period plots for (left) TXx5day, (middle) Rx1day and (right) annual maximum wind for (top) the British Isles, (2nd row) Scandinavia, (3rd row) Central Europe, (4th row) Southern Europe and (5th row) the Alps. Grey represents the N96 self-analogues, blue the N512 self-analogues, red is for N96 circulation with N512 variables (e.g. precipitation)**

1155 and green is for N512 circulation with N96 variables. Thin lines represent individual ensemble members, thick lines represent the mean across individual ensemble members. Blue dashed line represents the original N512 ensemble mean results like those shown in Figure 6 (although sometimes based on a different time period), and the grey dashed lines represent the equivalent for the N96 simulations. Results for TXx5day are based on the period 1985-2011, Rx1day 1986-2011, and wind 1986-2011.